Neuron

The nematode *C. elegans* senses airborne sound

Highlights

- Hearing is thought to only exist in vertebrates and some arthropods
- Here we show that the earless nematode *C. elegans* senses airborne sound
- Sound vibrates worm skin, activates sound-sensitive neurons, and triggers phonotaxis
- Worm sound-sensitive neurons transduce sound via nAChRs independently of ACh

Authors

Adam J. Iliff, Can Wang, Elizabeth A. Ronan, ..., Karl Grosh, R. Keith Duncan, X.Z. Shawn Xu

Correspondence

shawnxu@umich.edu

In brief

Hearing is thought to exist only in vertebrates and some arthropods, but not other animal phyla. Here, Xu and colleagues report that the earless nematode *C. elegans* senses airborne sound and engages in phonotaxis. Thus, hearing might have evolved multiple times independently in the animal kingdom, suggesting convergent evolution.

Iliff et al., 2021, Neuron *109*, 3633–3646
November 17, 2021
https://doi.org/10.1016/j.neuron.2021.08.035

CellPress

Neuron

CellPress
OPEN ACCESS

Article

The nematode *C. elegans* senses airborne sound

Adam J. Iliff,[1,2,7] Can Wang,[1,2,3,7] Elizabeth A. Ronan,[1,2] Alison E. Hake,[4] Yuling Guo,[1,2,3] Xia Li,[1,2] Xinxing Zhang,[1,2] Maohua Zheng,[1,2] Jianfeng Liu,[3] Karl Grosh,[4,5] R. Keith Duncan,[6] and X.Z. Shawn Xu[1,2,8,*]

[1]Life Sciences Institute, University of Michigan, Ann Arbor, MI 48109, USA
[2]Department of Molecular and Integrative Physiology, University of Michigan, Ann Arbor, MI 48109, USA
[3]College of Life Science and Technology, Key Laboratory of Molecular Biophysics of MOE, Huazhong University of Science and Technology, Wuhan, Hubei 430074, China
[4]Department of Mechanical Engineering, University of Michigan, Ann Arbor, MI 48109, USA
[5]Department of Biomedical Engineering, University of Michigan, Ann Arbor, MI 48109, USA
[6]Department of Otolaryngology-Head and Neck Surgery, University of Michigan, Ann Arbor, MI 48109, USA
[7]These authors contributed equally
[8]Lead contact
*Correspondence: shawnxu@umich.edu
https://doi.org/10.1016/j.neuron.2021.08.035

SUMMARY

Unlike olfaction, taste, touch, vision, and proprioception, which are widespread across animal phyla, hearing is found only in vertebrates and some arthropods. The vast majority of invertebrate species are thus considered insensitive to sound. Here, we challenge this conventional view by showing that the earless nematode *C. elegans* senses airborne sound at frequencies reaching the kHz range. Sound vibrates *C. elegans* skin, which acts as a pressure-to-displacement transducer similar to vertebrate eardrum, activates sound-sensitive FLP/PVD neurons attached to the skin, and evokes phonotaxis behavior. We identified two nAChRs that transduce sound signals independently of ACh, revealing an unexpected function of nAChRs in mechanosensation. Thus, the ability to sense airborne sound is not restricted to vertebrates and arthropods as previously thought, and might have evolved multiple times independently in the animal kingdom, suggesting convergent evolution. Our studies also demonstrate that animals without ears may not be presumed to be sound insensitive.

INTRODUCTION

To sense the external and internal world, animals and humans have evolved a wide array of sensory systems. Among the six common sensory modalities, the senses of vision, touch, olfaction, taste, and proprioception are all widespread in the animal kingdom and found in most, if not all, animal phyla (Ache and Young, 2005; Gehring, 2014; Mill, 1976; Prescott and Dürr, 2015; Wicher, 2012). For example, even simple organisms such as cnidarians are capable of sensing light, touch, and chemicals and also possess the sense of proprioception (Katsuki and Greenspan, 2013). Strikingly, the sense of hearing is found only in vertebrates and some arthropods (Budelmann, 1992; Faure et al., 2009; Webster, 1992). Most invertebrate species are, however, considered sound insensitive (Budelmann, 1992; Faure et al., 2009; Webster, 1992).

While hearing facilitates intraspecies communications, a more fundamental function of this sensory modality is to help the animal to locate predators and prey (Gans, 1992; Webster, 1992), which would benefit the survival of the animal, thereby increasing its fitness. As such, one might envision that hearing should have evolved more widely across animal phyla. However, it is difficult to test this concept, particularly in aquatic invertebrates, as it is technically challenging to distinguish among behavioral responses evoked by sound waves, substrate-borne vibrations, and local water movements (Budelmann, 1992).

The nematode *C. elegans* is widely used as a model for the study of sensory biology, because of its amenability to genetic manipulations and its small and well-annotated nervous system (Iliff and Xu, 2020). Furthermore, to survive the harsh environment, worms have evolved a rich repertoire of sensory systems. For example, worms are long known to have the senses of touch, olfaction, and taste (Bargmann et al., 1993; Bargmann and Horvitz, 1991; Chalfie et al., 1985; Ward, 1973). We and others recently reported that worms also possess the sense of light (Edwards et al., 2008; Ward et al., 2008), as well as proprioception (Li et al., 2006). However, as worms do not have morphologically distinct ear organs, these animals are presumed to be insensitive to airborne sound and thereby lack auditory sensation, which represents the only primary sensory modality absent in *C. elegans*.

Here, we found that despite the lack of ears, worms respond robustly to airborne sound at frequencies reaching the kHz range. Sound vibrates *C. elegans* skin that act as a sound pressure-to-displacement transducer similar to insect and vertebrate tympanum (eardrum), triggering the activation of sound-sensitive FLP and PVD neurons attached to the skin and evoking phonotaxis behavior. Interestingly, TRP and TMC mechanotransduction channels that mediate auditory sensation

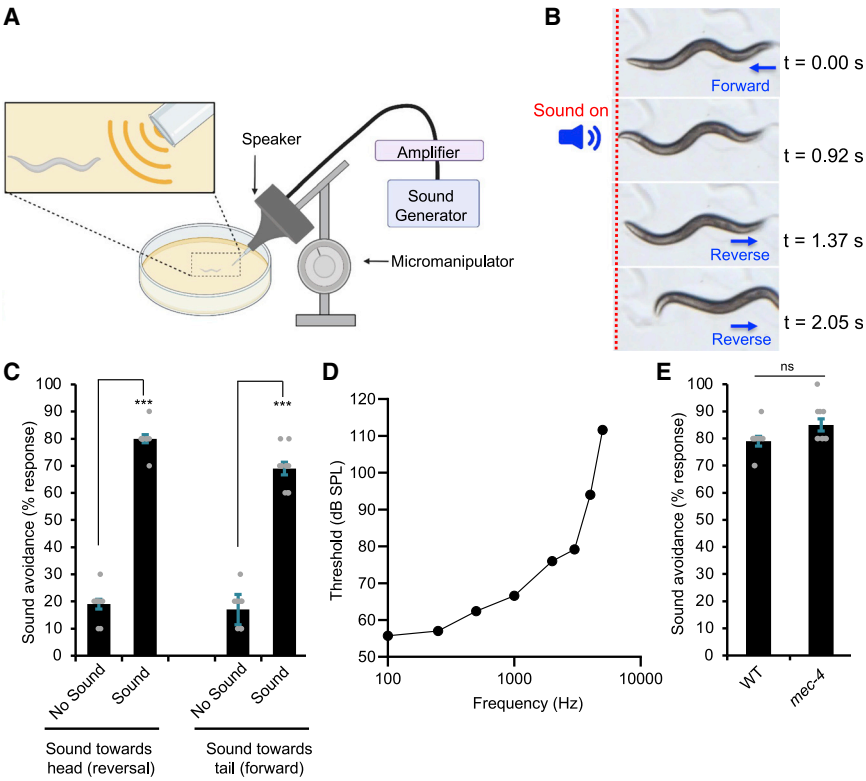

Figure 1. Sound evokes aversive phonotaxis behavior in *C. elegans* in a frequency-dependent manner

(A) Schematic describing the assay. The speaker was mounted on a micromanipulator and fitted with an output port, a configuration that allows one to deliver sound stimuli to specific body parts of the worm (e.g., head versus tail) under a stereomicroscope. Speaker output was carefully calibrated with a mini-microphone to accurately reflect the sound pressure levels (SPLs) received by the worm. See STAR Methods for details.

(B) Snapshot images showing that sound stimuli triggered an avoidance response in a worm moving forward. A brief pulse of sound (2 s, 1 kHz, 80 dB SPL) was delivered to the head of the worm. The animal immediately halted forward locomotion and initiated a reversal. The dotted red line indicates the position of the worm in the field.

(C) Worms avoid sound sources. The low basal response in the control groups arose from spontaneous reversals or acceleration of forward movement. ***$p < 0.0001$ (t test). $n \geq 10$.

(D) Worms respond to sound in a frequency-dependent manner. Sound stimuli (2 s) of varying frequency and SPL were tested for the head-avoidance phonotaxis behavior. Threshold was defined as the SPL of the stimulus that triggered a 50% response rate.

(E) *mec-4(e1611)* mutant worms show no defect in phonotaxis behavior. $p > 0.05$ (t test). $n \geq 10$.

All error bars denote SEM. See also Figure S1.

in insects and vertebrates, respectively, are not required to transduce sound signals in FLP/PVD neurons in *C. elegans*. In an activity-based forward genetic screen, we instead identified two nAChR (nicotinic acetylcholine receptor) subunits that are required for transducing sound signals, and surprisingly, this role of nAChRs is independent of their function as acetylcholine (ACh) receptors. Further analysis suggests that these two nAChRs function as essential subunits of the sound transduction channel. Thus, the ability to sense airborne sound is not restricted to vertebrates and arthropods as previously thought, suggesting that auditory sensation might have evolved multiple times independently in the animal kingdom. Our work also uncovers an unexpected ACh-independent function of nAChRs in mechanosensation and indicates that animals without ears may not be presumed to be insensitive to sound. This raises the intriguing possibility that other invertebrate animals with soft bodies similar to *C. elegans*, such as terrestrial mollusks, annelids, and flatworms, might also be capable of sensing airborne sound.

RESULTS

Sound evokes aversive phonotaxis behavior in a frequency-dependent manner

C. elegans was previously thought to live in the soil. However, recent work showed that *C. elegans* in fact lives in composts and rotting materials above ground (Félix and Braendle, 2010), suggesting that they are more vulnerable to some of their predators (e.g., arthropods) (Kiontke and Fitch, 2013), whose activities produce audible sound. We thus reasoned that worms might exhibit aversive behavioral responses to audible sound. Given the small size of the worm, we developed a system that allowed us to deliver sound stimuli from a speaker to specific body parts of the worm, for example, head versus tail (Figure 1A). We found that worms responded robustly to sound stimuli (Figures 1B, 1C, and S1A). Specifically, sound stimuli (2 s, 1 kHz, 80 dB sound pressure level [SPL]) delivered to the head stopped worms from moving forward and triggered backward movement (reversals) (Figures 1B, 1C, and S1A; Video S1). When we aimed the speaker at the tail of the worm, sound stimuli stimulated forward movement (Figures 1C and S1A; Video S2). Thus, worms avoid sound sources, exhibiting aversive phonotaxis behavior. This also demonstrates that worms are able to locate sound sources. As it is much easier to score reversals, we decided to focus on characterizing the head-avoidance phonotaxis behavior (sound-evoked reversals).

We examined phonotaxis responses triggered by different frequencies of sound (Figure 1D). Worms responded to sound at frequencies spanning from 100 Hz to 5 kHz (Figure 1D), a range that is even broader than some vertebrate animals (e.g., most fishes and turtles) (Christensen-Dalsgaard et al., 2012; Schellart and Popper, 1992). The activation threshold, which is defined as the sound intensity needed to trigger phonotaxis responses, varied with sound frequencies, reaching the range of 50–60 dB SPL at low frequencies (Figure 1D). We did not test frequencies below 100 Hz, because of limitations of the speaker setup. At frequencies above 5 kHz, no response was detected at the maximum stimulus intensity possible in our setup (~110 dB

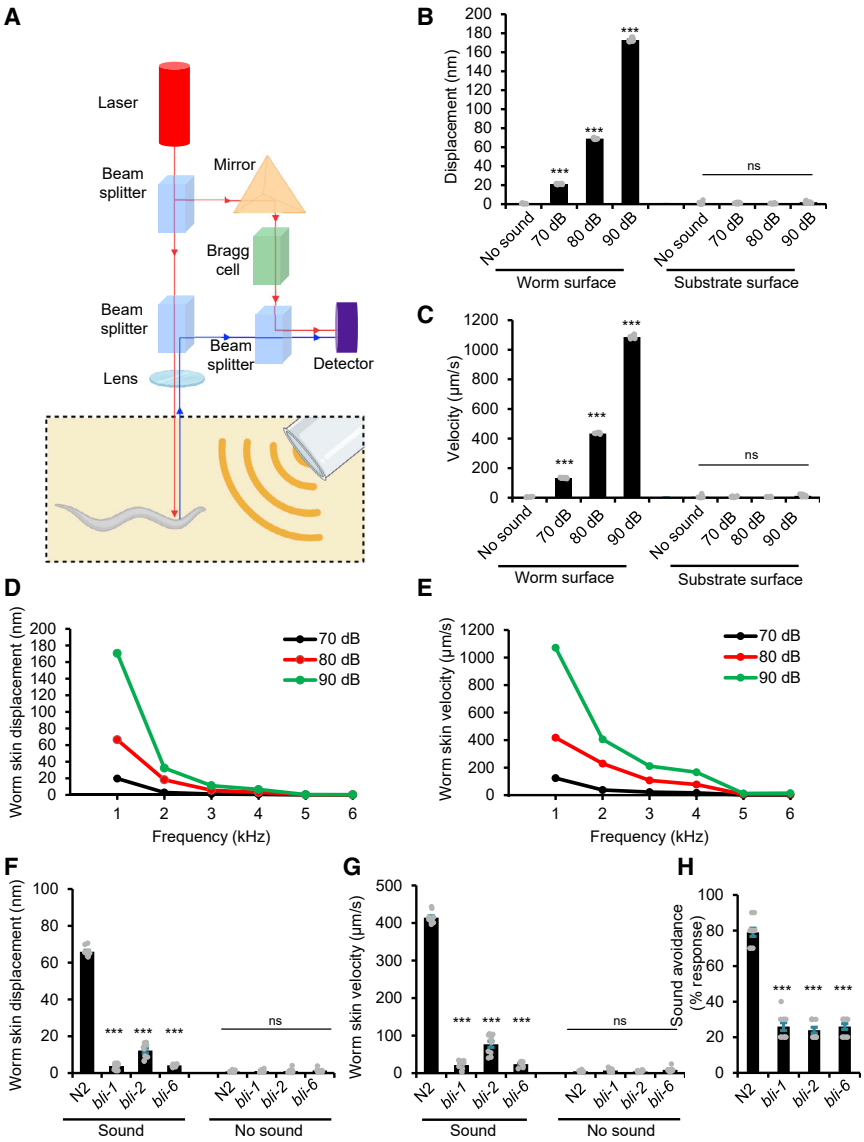

Figure 2. Airborne sound vibrates *C. elegans* skin to trigger phonotaxis behavior

(A) Schematic describing the laser Doppler vibrometry system used to measure non-contact surface vibration. The laser beam was directed at the surface of either the anterior region of the worm or the agar substrate. The vibration amplitude and frequency were extracted from the Doppler shift of the reflected laser beam frequency caused by surface vibration.

(B and C) Displacement and velocity values of sound-evoked vibrations. Sound (1 kHz) at the specified sound pressure levels (SPLs) was applied. (B) Displacement graph. (C) Velocity graph. ***$p < 0.0001$ (ANOVA with Bonferroni test). $n \geq 10$.

(D and E) Displacement and velocity values of agar surface vibrations evoked by sounds of varying frequencies. Sound frequencies lower than 1 kHz were not tested because of limitations of the system. (D) Worm skin displacement plot. (E) Worm skin velocity plot. $n \geq 10$.

(F and G) *bli* mutants show a strong defect in sound-evoked vibrations in the cuticle. Worms were tested with 1 kHz sound (80 dB SPL). (F) Worm skin displacement graph. (G) Worm skin velocity graph. ***$p < 0.0001$ (ANOVA with Bonferroni test). $n \geq 10$

(H) *bli* mutants are defective in phonotaxis behavior. Head-avoidance responses were tested (2 s, 1 kHz at 80 dB SPL). ***$p < 0.0001$ (ANOVA with Bonferroni). $n \geq 10$.

All error bars denote SEM. See also Figure S2.

SPL). We thus conclude that worms respond to sound stimuli in a frequency-dependent manner. For convenience, we chose to use 1 kHz sound in further characterizations.

Phonotaxis behavior is activated by airborne sound rather than substrate-borne vibrations

As worms were tested on the surface of an agar plate, the substrate on which they navigate, one potential concern is that sound might vibrate the surface of the agar plate, and such substrate-borne vibrations would then trigger behavioral responses in worms. If so, worms might have responded to sound-evoked substrate-borne vibrations rather than airborne sound. Indeed, it is well known that substrate-borne vibrations trigger behavioral responses in worms (Holbrook and Mortimer, 2018; Wicks and Rankin, 1995). This mechanosensory behavior (i.e., tap responses) has been well characterized, which is mediated by touch receptor neurons (Wicks and Rankin, 1995). We thus tested *mec-4(e1611)* mutant worms in which touch receptor neurons are degenerated (Driscoll and Chalfie, 1991). *mec-4* mutant worms lacked substrate-borne vibration-activated behavior (Figure S1B), yet they exhibited normal phonotaxis behavior (Figure 1E), suggesting that phonotaxis is evoked by airborne sound rather than substrate-borne vibrations.

To provide further evidence, we directly measured sound-evoked substrate vibrations by laser Doppler vibrometry (Figure 2A). Specifically, we quantified the vibration parameters (i.e., displacement and velocity) of the surface layer of the agar plate. A displacement in the micrometer range is required to activate touch receptor neurons that mediate substrate-borne vibration-activated behavior (Eastwood et al., 2015). However, we detected minimal, if any, sound-evoked vibrations on the surface of the agar plate (Figures 2B and 2C). This provides further evidence suggesting that phonotaxis behavior is activated by airborne sound rather than substrate-borne vibrations.

Sound vibrates *C. elegans* skin to trigger phonotaxis behavior

We then asked how airborne sound activates phonotaxis behavior. In vertebrates and some insects, sound vibrates the tympanum (eardrum), triggering a wide range of auditory behavioral

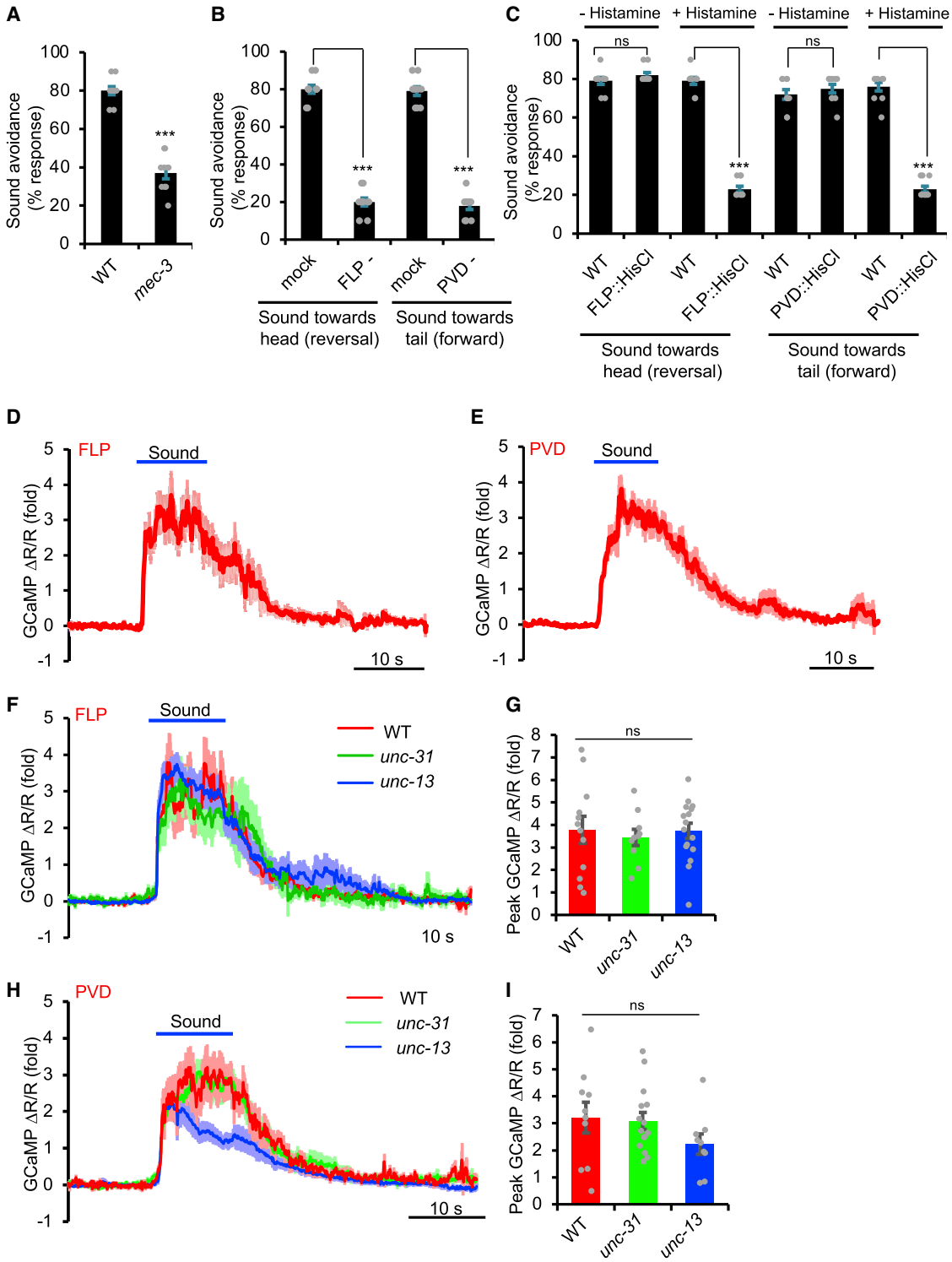

Figure 3. FLP and PVD neurons are sound-sensitive neurons mediating phonotaxis behavior

(A) *mec-3(e1338)* mutant worms are defective in phonotaxis behavior. Head-avoidance response was tested. Sound stimulus: 2 s, 1 kHz at 80 dB SPL. ***$p < 0.0001$ (t test). $n \geq 10$.

(B) Laser ablation of FLP and PVD neurons leads to a severe defect in sound-evoked reversals and forward movement, respectively. ***$p < 0.0001$ (t test). $n \geq 10$.

(C) Acute silencing of FLP and PVD neurons with a HisCl transgene leads to a severe defect in sound-evoked reversals and forward movement, respectively. ***$p < 0.0001$ (t test). $n \geq 10$.

(legend continued on next page)

responses (Christensen-Dalsgaard and Carr, 2008; Göpfert and Hennig, 2016). In this case, the eardrum functions as a pressure-to-displacement transducer, converting sound pressure waves into mechanical motion. *C. elegans* body is covered by the cuticle, a thin (<1 μm thickness), elastic membrane composed primarily of collagen (Bercher et al., 2001; Cohen and Sundaram, 2020). Using laser Doppler vibrometry, we found that the surface of worm cuticle was actively vibrated by sound (Figures 2B and 2C; Figures S2A–S2D). For example, in response to 1 kHz sound stimulus, the cuticle vibrated at the same 1 kHz frequency (Figures S2A and S2B). Further analysis showed that the displacement and velocity of sound-evoked cuticle vibrations decreased as the sound frequency increased (Figures 2D and 2E). No vibrations were detected in the cuticle in response to sound at frequencies of >5 kHz (Figures 2D and 2E), consistent with our phonotaxis behavior data (Figure 1D). These results demonstrate that sound waves can actively vibrate *C. elegans* cuticle.

It should be noted that although sound vibrates the cuticle, this type of mechanical stimulus is rather mild, as the cuticle displacement caused by sound stimulation is in the nanometer range (Figure 2D). Notably, when evoked by high-frequency sounds (e.g., 3 kHz, 80 dB SPL sound; Figure 2D), a cuticle displacement as small as ~5 nm was sufficient to trigger phonotaxis responses (Figure 1D). By contrast, a micrometer range of cuticle displacement is required for other types of mechanical stimuli, such as gentle touch, to activate mechanosensory behavioral responses in *C. elegans* (Eastwood et al., 2015).

Are sound-evoked cuticle vibrations important for phonotaxis behavior? To address this question, we set out to test mutants with aberrant cuticle structure, as they may display a defect in sound-evoked vibrations in the cuticle. We focused on *bli-1*, *2*, and *6* mutants. Unlike other cuticle mutants that largely maintain normal layered cuticle structure, these three cuticle mutants lack struts in the intermediate layer of the cuticle and display disrupted cuticle structure with the cortical and basal layers detached from each other (Cohen and Sundaram, 2020). We found that *bli-1*, *2*, and *6* mutants exhibited a strong defect in sound-evoked vibrations in the cuticle (Figures 2F and 2G). Importantly, these cuticle mutants were severely defective in sound-evoked phonotaxis behavior (Figure 2H), though they responded to other aversive cues, such as osmotic shock (Figure S2E). These results together demonstrate that sound vibrates *C. elegans* cuticle, which is essential for triggering phonotaxis behavior.

FLP and PVD neurons are sound-sensitive neurons mediating phonotaxis behavior

Sound is expected to activate sound-sensitive mechanosensory neurons to drive phonotaxis behavior. To identify such sound-sensitive neurons, we examined *mec-3* mutant worms in which several classes of mechanosensory neurons fail to differentiate properly (Way and Chalfie, 1989), and found that these mutant worms were defective in phonotaxis behavior (Figure 3A). Notably, *mec-4* mutants did not express such a phonotaxis phenotype (Figure 1E). The difference between *mec-3* and *mec-4* mutants is that the former but not the latter affects FLP and PVD neurons (Way and Chalfie, 1989), two mechanosensory neurons known to be activated by noxious touch and body stretch (Albeg et al., 2011; Li et al., 2011; Tao et al., 2019). Activation of FLP and PVD neurons triggers reversals and forward movement, respectively (Husson et al., 2012; Li et al., 2011). These features together suggest FLP and PVD neurons as candidate sound-sensitive neurons mediating sound-evoked reversals and forward movement, respectively. Indeed, worms with FLP and PVD neurons ablated using a laser micro-beam exhibited severe defects in sound-evoked reversals and forward movement, respectively (Figure 3B), suggesting that these neurons are required for phonotaxis behavior. To provide additional evidence, we acutely silenced FLP and PVD neurons with a HisCl transgene, which encodes a histamine-gated Cl^- channel (Pokala et al., 2014), and found that such acute silencing of FLP and PVD yielded a similar defect (Figure 3C). These results demonstrate that FLP and PVD neurons are required for mediating phonotaxis behavior, suggesting that they are sound-sensitive neurons.

To garner further evidence, we recorded the activity of FLP and PVD neurons in response to sound stimuli by calcium imaging. Considering the mechanosensory nature of FLP and PVD neurons, we imaged freely moving rather than immobilized worms, as immobilization may generate mechanical stresses affecting these neurons. We found that sound evoked robust calcium responses in FLP and PVD neurons (Figures 3D, 3E, and S3). We repeated the experiments in *unc-13* and *unc-31* mutant worms that are devoid of neurotransmission mediated by exocytosis from synaptic vesicles (SVs) and dense core vesicles (DCVs), respectively (Richmond et al., 1999; Speese et al., 2007). Sound-evoked calcium responses persisted in FLP neurons of *unc-13* and *unc-31* mutant worms (Figures 3F and 3G). A similar result was obtained with PVD neurons, though the response was slightly reduced in *unc-13* worms (Figures 3H and 3I). Thus, the observed responses in FLP and PVD neurons likely arose cell-autonomously, suggesting that FLP and PVD neurons are primary sound-sensitive neurons mediating phonotaxis behavior. As we focused on the head-avoidance phonotaxis behavior (sound-evoked reversals) mediated by FLP neurons, we decided to focus on recording FLP neurons in further characterizations.

(D and E) FLP and PVD neurons are sound sensitive. Sound evoked robust calcium responses in FLP (D) and PVD (E) neurons. Worms carried a transgene expressing GCaMP6 in FLP or PVD neurons using the *sto-5* or *ser-2(prom3)* promoter, respectively (Russell et al., 2014; Tsalik et al., 2003). mCherry was co-expressed with GCaMP6f to enable ratiometric imaging. Sound stimulus: 10 s, 1 kHz at 89 dB SPL. Shown are averaged traces. Shades along the traces indicate error bars (SEM). $n \geq 10$.

(F and G) Sound-evoked FLP calcium responses persist in *unc-13* and *unc-31* mutant backgrounds. (F) Average traces. (G) Bar graphs. $p > 0.05$ (ANOVA with Bonferroni test). $n \geq 10$.

(H and I) Sound-evoked PVD calcium responses persist in *unc-13* and *unc-31* mutant backgrounds. (H) Average traces. (I) Bar graphs. Responses in *unc-13* mutant background were slightly reduced, though such a reduction was not statistically significant. $p > 0.05$ (ANOVA with Bonferroni test). $n \geq 10$.

All error bars denote SEM. See also Figure S3.

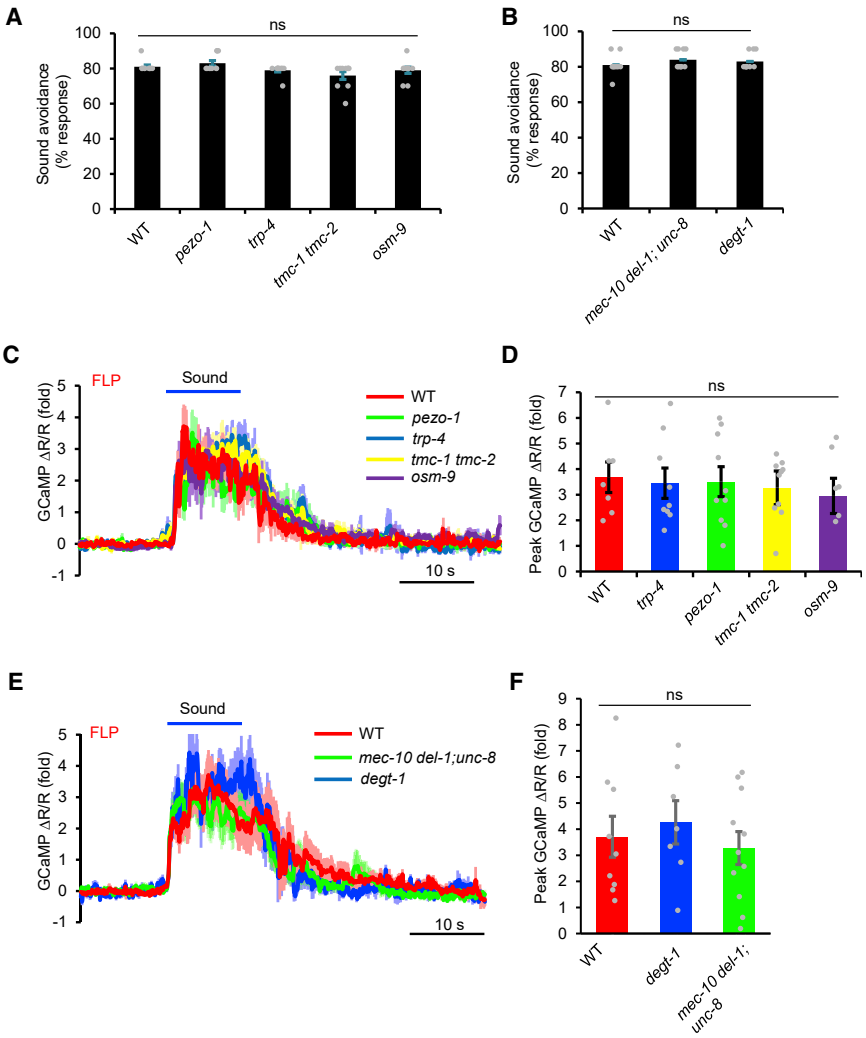

Figure 4. Known mechanotransduction channels are not required for auditory sensation in *C. elegans*.

(A) TRP, TMC, and Piezo channel mutants show no defect in phonotaxis behavior. Sound-evoked head-avoidance response was tested. Sound stimulus: 2 s, 1 kHz at 80 dB SPL. $p > 0.05$ (ANOVA with Bonferroni test). $n \geq 10$.

(B) Mutants lacking the harsh touch-sensitive DEGT-1 and stretch-sensitive MEC-10/DEL-1/UNC-8 channels do not show a defect in phonotaxis behavior. $p > 0.05$ (ANOVA with Bonferroni test). $n \geq 10$.

(C and D) TRP, TMC, and Piezo channel mutants show no defect in sound-evoked calcium responses in FLP neurons. (C) Average traces. (D) Bar graph. $p > 0.05$ (ANOVA with Bonferroni test). $n \geq 10$

(E and F) DEGT-1 and MEC-10/DEL-1/UNC-8 channel mutants show no defect in sound-evoked calcium responses in FLP neurons. (E) Average traces. (F) Bar graphs. $p > 0.05$ (ANOVA with Bonferroni test). $n \geq 10$

All error bars denote SEM.

Known mechanotransduction channels are not required for auditory sensation in *C. elegans*

Having identified sound-sensitive neurons driving phonotaxis behavior, we next sought to identify the mechanotransduction channel(s) that transduces sound signals in these neurons. In insects and vertebrates, TRP (TRPN/NOMPC and TRPV) and TMC mechanotransduction channels transduce sound signals in sound-sensitive chordotonal neurons and inner ear hair cells, respectively (Göpfert and Hennig, 2016; Jia et al., 2020; Pan et al., 2013). Mutant worms lacking the *C. elegans* TRPN/NOMPC channel TRP-4 and TRPV channel OSM-9 showed normal phonotaxis behavior (Figure 4A). FLP neurons also responded normally to sound stimulation in *trp-4* and *osm-9* mutant worms (Figures 4C and 4D). *C. elegans* encodes two TMC channels: TMC-1 and TMC-2 (Wang et al., 2016); however, no defect in phonotaxis behavior or sound-evoked calcium responses was detected in *tmc-1 tmc-2* double-mutant worms (Figures 4A, 4C, and 4D). Thus, *C. elegans* sound sensing in FLP neurons appears to require mechanotransduction channels distinct from those found in insects and vertebrates.

We also examined several other mechanotransduction channels, for example, the Piezo channel PEZO-1, but did not observe any defect in *pezo-1* mutant worms (Figures 4A, 4C, and 4D). As FLP/PVD neurons are also activated by harsh touch and body stretch, we tested the corresponding mechanotransduction channels DEGT-1 and UNC-8/MEC-10/DEL-1, which are activated by these two types of mechanical stimuli, respectively (Tao et al., 2019). No defect was observed in *degt-1* and *unc-8; mec-10 del-1* mutant worms (Figures 4B, 4E, and 4F). We thus conclude that *C. elegans* sound-sensitive FLP/PVD neurons require a distinct type of mechanotransduction channel(s) to transduce sound signals.

An unbiased, activity-based genetic screen identifies two nAChR subunits, DES-2 and DEG-3, required for auditory sensation

The failure to identify mechanotransduction channels that transduce sound signals in *C. elegans* with candidate gene approaches prompted us to consider an unbiased strategy. We thus opted to perform an unbiased forward genetic screen. We first followed the traditional strategy by performing a chemical-mutagenesis screen for mutants defective in phonotaxis behavior. However, this screen did not turn out to be very fruitful, as further characterizations of FLP neurons by calcium imaging revealed that the majority of isolated mutants did not show a defect in FLP neurons. This might be explained by the fact that behavioral screens usually lack specificity. Thus, the phenotype observed in the mutants might simply result from defects in sensory processing mediated by downstream neural circuits rather

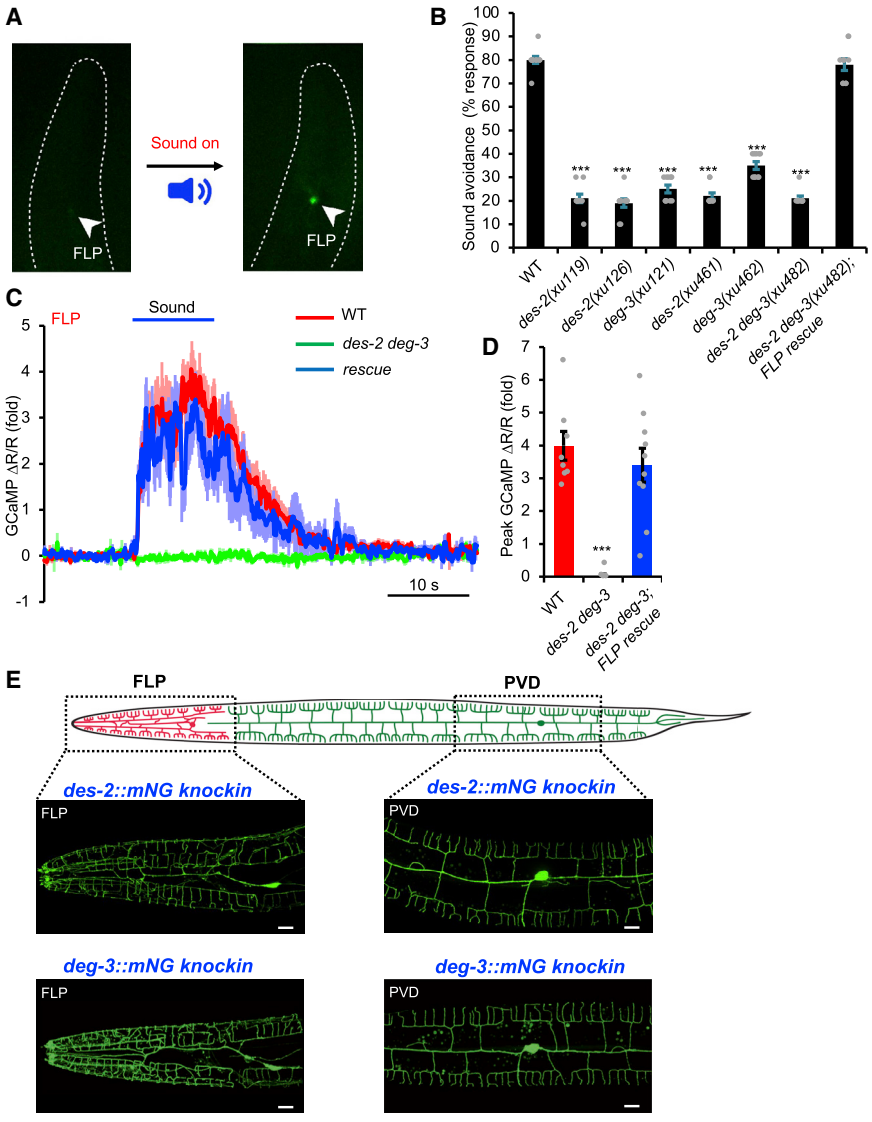

Figure 5. An unbiased, activity-based genetic screen identifies two nAChR subunits DES-2 and DEG-3 that are required for auditory sensation in *C. elegans*

(A) Design of the screen. Left panel: a transgenic worm expressing GCaMP6 showed a very low level of basal fluorescence in FLP neuron. Right panel: upon sound simulation, FLP fluorescence intensity in the same worm increased drastically. Images were taken under a fluorescence stereomicroscope from a freely moving worm placed in an NGM plate. Arrowheads point to FLP.

(B) *des-2 deg-3* mutant worms show a severe defect in phonotaxis behavior. Head-avoidance responses were tested. *des-2 deg-3* mutant phenotype was rescued with wild-type *des-2* and *deg-3* cDNA expressed as a transgene in FLP neurons. See STAR Methods for the molecular lesions in mutant alleles. ***$p < 0.0001$ (ANOVA with Bonferroni test). $n \geq 10$.

(C and D) FLP neurons in *des-2 deg-3* mutant worms do not show sound-evoked calcium responses, a phenotype rescued by transgenic expression of wild-type *des-2* and *deg-3* genes in FLP neurons. (C) Average traces. Shades along the traces indicated error bars (SEM). (D) Bar graph. ***$p < 0.0001$ (ANOVA with Bonferroni test). $n \geq 10$.

(E) DES-2 and DEG-3 are expressed in FLP and PVD neurons. Shown in the top panel is a schematic illustrating the morphology of FLP and PVD neurons. Shown in the lower panels are confocal images of *des-2::mNG* and *deg-3::mNG* knockin worms. Scale bars, 10 μm.

All error bars denote SEM. See also Figure S4.

than in sound sensing by FLP neurons. We thus sought to design an activity-based genetic screen by directly targeting the sound-sensitive neuron FLP.

We made the intriguing observation that FLP neurons maintained a low basal level of GCaMP fluorescence at the quiescent state but responded robustly to sound stimulation by drastically increasing their GCaMP fluorescence intensity (Figure 5A). This enabled us to conduct a genetic screen by visually screening for mutants in which GCaMP fluorescence intensity in FLP failed to increase upon sound stimulation under a stereomicroscope. After screening ~20,000 F2 worms, we isolated 13 mutants. We focused on 3 strong mutants: *xu119*, *xu121*, and *xu126*. As expected, these mutants were also defective in phonotaxis behavior (Figure 5B). By whole-genome sequencing, we mapped *xu119* and *xu126* to the *des-2* gene and *xu121* to the *deg-3* gene. *des-2* and *deg-3* encode two nAChR subunits that function together as a heteromeric channel (Treinin et al., 1998). These two genes are encoded by the same operon (Treinin et al., 1998). To validate the phenotype, we examined null mutants (deletion alleles) generated using CRISPR-based genome editing. Null mutants, including *des-2* and *deg-3* single mutants (*des-2[xu461]* and *deg-3[xu462]*) as well as *des-2 deg-3* double mutant (*des-2 deg-3[xu482]*), all exhibited the same phonotaxis phenotype (Figure 5B). In contrast, *des-2 deg-3* mutant worms showed normal responses in other aversive behaviors, such as tap response, osmotic avoidance, and nose touch response (Figures S1B, S4A, and S4B). We then focused on *des-2 deg-3* double mutant for further characterizations. We recorded FLP neurons in *des-2 deg-3* mutant worms using calcium imaging and found that they failed to respond to sound (Figures 5C and 5D). Transgenic expression of wild-type (WT) *des-2* and *deg-3* genes in FLP neurons rescued both the phonotaxis behavior and calcium imaging phenotypes (Figures 5B–5D), indicating that DES-2/DEG-3 acts in FLP neurons to mediate sound sensing.

To determine the expression pattern of DES-2/DEG-3, we inserted an mNeonGreen (mNG) tag into the endogenous locus of *des-2* and *deg-3* using CRISPR-based genome editing. Both *des-2::mNG* and *deg-3::mNG* knockin alleles were functional, as they responded normally to sound stimuli (Figures S4C–S4E), indicating that the mNG tag does not interfere with the function of DES-2/DEG-3. As described previously (Albeg

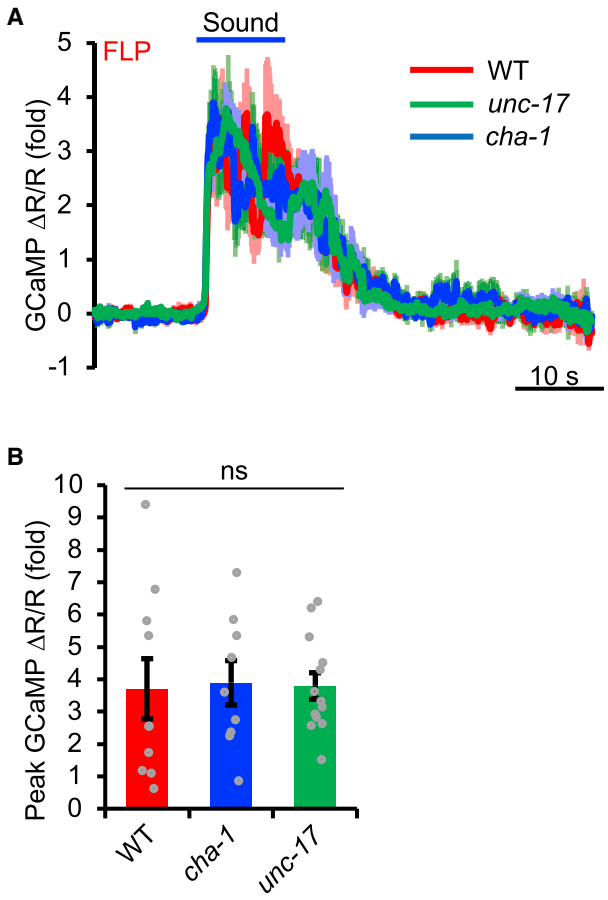

Figure 6. Acetylcholine (ACh) is not required for the function of DES-2/DEG-3 in auditory sensation

(A and B) *cha-1* and *unc-17* mutants lack the synthesis and release of ACh, respectively. FLP neurons in these two mutant worms responded normally to sound. (A) Average calcium imaging traces. Shades along the traces denote error bars (SEM). (B) Bar graphs. Error bars denote SEM. $p > 0.05$ (ANOVA with Bonferroni test). $n \geq 10$.

et al., 2011), we found that DES-2 and DEG-3 were expressed throughout the sensory dendrites and soma of FLP neurons (Figure 5E). DES-2 and DEG-3 were also expressed strongly in PVD neurons and weakly in a few other neurons (Figures 5E and S4F). Indeed, similar to FLP neurons, PVD neurons in *des-2 deg-3* mutant worms also failed to respond to sound (Figures S4G–S4I). Among all the worm neurons, FLP and PVD are unique in that they are multi-dendritic neurons with their dendritic trees covering the head and body/tail of the worm, respectively, and together these two sound-sensitive neurons tile the entire body wall of the worm (Figure 5E) (Albeg et al., 2011; Inberg et al., 2019; Sundararajan et al., 2019). Notably, FLP/PVD soma are positioned apposed to the epidermis, and their dendrites are physically attached to the epidermis (Inberg et al., 2019; Sundararajan et al., 2019), a morphological feature that is well suited to detect sound-evoked vibrations in the skin. Thus, it appears that both the morphology of FLP/PVD neurons and the expression pattern of DES-2/DEG-3 channels are consistent with their roles in mediating sound sensing in *C. elegans*.

ACh is not required for the function of DES-2/DEG-3 in auditory sensation

The identification of the nAChR DES-2/DEG-3 as an essential player in sound sensing raises the question about the specific role of DES-2/DEG-3 in this sensory modality. As DES-2/DEG-3 is an ACh-gated ion channel (Treinin et al., 1998), it is conceivable that sound stimuli might somehow stimulate ACh release, which in turn would activate the nAChR DES-2/DEG-3. If so, DES-2/DEG-3 would play a rather indirect role in the process. Indeed, DES-2/DEG-3 has been reported to indirectly regulate mechanosensation in an ACh-dependent manner (Cohen et al., 2014). In this case, one would expect that ACh should be important for sound sensing and that inhibiting the synthesis or release of ACh will recapitulate the *des-2 deg-3* mutant phenotype. To test this model, we examined *cha-1* and *unc-17* mutant worms that are deficient in ACh synthesis and release, respectively. Specifically, *cha-1* and *unc-17* encode the worm ortholog of choline acetyltransferase (ChAT) and vesicular ACh transporter (VAChT), respectively, with the former being essential for ACh synthesis and the latter required for uploading ACh to SVs and hence ACh release (Alfonso et al., 1993, 1994). To our surprise, both *cha-1* and *unc-17* mutants exhibited normal sound-evoked responses in FLP neurons (Figures 6A and 6B), indicating that ACh is not required for sound sensing. Thus, though DES-2/DEG-3 has the capacity to function as an ACh receptor, its ACh receptor function does not contribute to sound sensing, suggesting that DES-2/DEG-3 may play a more direct role in auditory sensation in *C. elegans*. This also uncovers an ACh-independent function of nAChRs.

DES-2/DEG-3 is an essential component of the sound transduction channel

The lack of a role for the ACh receptor function of DES-2/DEG-3 in sound sensing prompted us to ask how DES-2/DEG-3 is involved. In addition to acting as an ACh receptor, nAChRs are also ion channels. We thus wondered if the ion channel function of DES-2/DEG-3 is important for sound sensing. The transmembrane segment M2 lines the channel pore of nAChRs. The point mutations G243K and A258R in the M2 segment in mammalian nAChRs (e.g., α7 nAChR) are known to abolish the channel conductance (Criado et al., 2011). The corresponding point mutations are G277K and S292R in DES-2 and G305K and S320R in DEG-3 (Figure S5A). We recorded agonist-evoked currents of DES-2/DEG-3 expressed in HEK293T cells and verified that these mutant forms of DES-2/DEG-3 lacked channel activity even in response to prolonged agonist application (Figures S5B and S5D). No reliable mechanically activated currents were recorded in DES-2/DEG-3 expressed in HEK293T cells (Figure S5C). These *in vitro* data, however, do not necessarily indicate that this channel is mechano-insensitive, as some of the auxiliary proteins required for DES-2/DEG-3 mechanosensitivity *in vivo* may be absent in HEK293T cells *in vitro*. A similar phenomenon was observed with the mechanosensitive ENaC/DEG channel subunits MEC-4/MEC-10 when expressed *in vitro* (Bounoutas and Chalfie, 2007; Goodman et al., 2002). We then tested those channel-dead mutant forms of DES-2/DEG-3 in worms by expressing them as a transgene in FLP neurons and found that they failed to rescue the phonotaxis

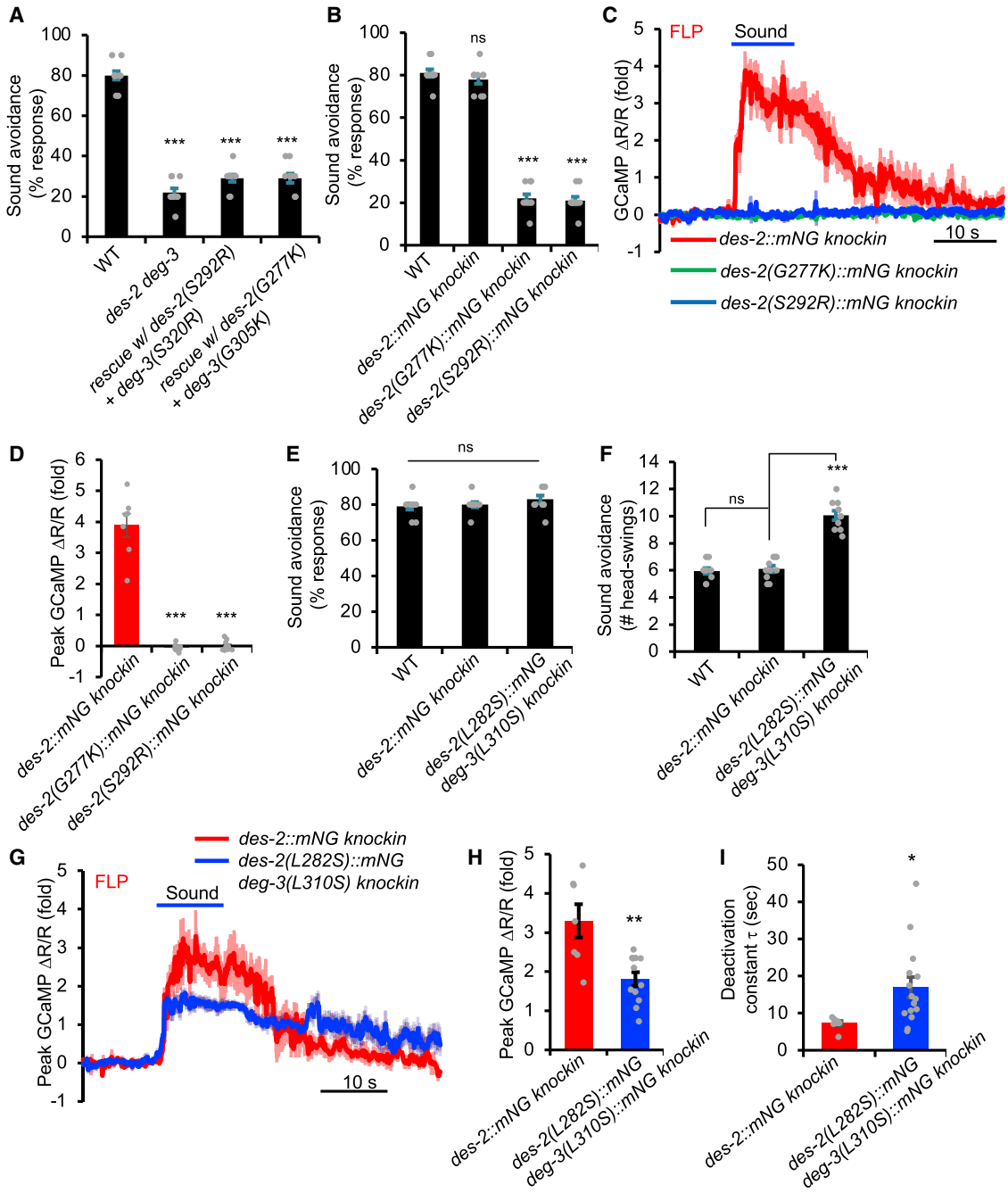

Figure 7. DES-2/DEG-3 is an essential component of the sound transduction channel

(A) Channel-dead mutant forms of DES-2/DEG-3 fail to rescue *des-2 deg-3* phonotaxis mutant phenotype. Transgenes were expressed in *des-2 deg-3* mutant background. Head-avoidance phonotaxis behavior was tested. ***$p < 0.0001$ (ANOVA with Bonferroni test). $n \geq 10$.

(B) *des-2(G277K)* and *des-2(S292R)* knockin worms carrying channel-dead mutations are severely defective in phonotaxis behavior. G277K and S292R mutations were introduced into *des-2::mNG* knockin background by CRISPR. ***$p < 0.0001$ (ANOVA with Bonferroni test). $n \geq 10$. Note that in *des-2::mNG* knockin worms, the *deg-3* locus was left intact. *deg-3* should also be functionally expressed in *des-2::mNG* knockin worms, as these knockin worms and their FLP neurons responded normally to sound in phonotaxis behavior and calcium imaging assays, respectively (Figures S4C–S4E).

(C and D) FLP neurons in *des-2(G277K)* and *des-2(S292R)* knockin worms, which carry channel-dead mutations, do not respond to sound. (C) Average calcium imaging traces. Shades along the traces denote error bars (SEM). (D) Bar graph. ***$p < 0.0001$ (ANOVA with Bonferroni test). $n \geq 10$

(E and F) Knockin worms carrying mutations that enhance the channel function of DES-2/DEG-3 respond more robustly to sound in phonotaxis behavior. The L-S mutation L282S and L310S was introduced into the endogenous *des-2* and *deg-3* locus using CRISPR, respectively. Although the response rate in L-S knockin

(legend continued on next page)

phenotype of *des-2 deg-3* mutant worms (Figure 7A), while a transgene expressing wild-type DES-2/DEG-3 did (Figure 5B). This suggests that the ion-conducting activity of DES-2/DEG-3 is required for its function in auditory sensation.

To provide additional evidence, we introduced the channel-dead mutations G277K and S292R into the endogenous *des-2* locus using CRISPR-based genome editing to generate two knockin alleles: *des-2(G277K)* and *des-2(S292R)*. We performed the genome editing in the *des-2::mNG* background, as the mNG (mNeonGreen) tag did not affect DES-2 function (Figures S4C–S4E), yet offered an opportunity to assess the potential effect of G277K and S292R mutations on DES-2 expression. As expected, these two channel-dead mutations did not notably affect the expression of the endogenous DES-2 protein (Figure S6). Importantly, *des-2(G277K)* and *des-2(S292R)* knockin worms, both of which carried channel-dead mutations, were severely defective in phonotaxis behavior (Figure 7B) and also completely lacked sound-evoked calcium responses in FLP neurons (Figures 7C and 7D), a phenotype identical to *des-2 deg-3* null mutant worms. This result provides strong evidence that the ion channel function of DES-2/DEG-3 is essential for transducing sound signals, suggesting that DES-2/DEG-3 is an essential component of the sound transduction channel.

To provide further evidence, we sought to perform the converse experiment by potentiating the channel activity of DES-2/DEG-3. We reasoned that if DES-2/DEG-3 is an essential component of the sound transduction channel, then potentiating its channel activity should potentiate the phonotaxis behavior and the sound-evoked activity of sound-sensitive neurons. The L-S point mutation (L248S in Figure S5A) in the pore-lining M2 segment of mammalian α7 nAChR is known to slow down the channel's desensitization/inactivation kinetics, thereby prolonging the open duration of the channel (Labarca et al., 1995; Revah et al., 1991). We first verified this result in HEK293T cells and found that DES-2/DEG-3 carrying the corresponding L-S mutation (DES-2[L282S]/DEG-3 [L310S]) inactivated much more slowly and thus remained open much longer than WT channel, though its amplitude was slightly reduced (Figures S5B, S5D, and S5E). We then introduced this L-S point mutation into the endogenous *des-2 deg-3* locus using CRISPR-based genome editing. In phonotaxis behavior tests, knockin worms carrying the L-S mutation in DES-2/DEG-3, although displaying a response rate similar to WT worms (Figure 7E), responded with more head swings (i.e., longer reversal distance) in each reversal event (Figure 7F), indicating that these knockin worms responded more robustly to sound stimuli. A similar phenomenon was observed in sound-evoked calcium responses in FLP neurons. Specifically, though the amplitude of sound-evoked calcium responses was reduced in L-S knockin worms (Figures 7G and 7H), upon the cessation of sound stimuli, the responses deactivated at a much slower pace than in WT worms (Figures 7G and 7I). This provides a neural basis underlying the enhanced phonotaxis behavioral responses in L-S knockin worms. Thus, enhancing the channel activity of DES-2/DEG-3 potentiated the phonotaxis behavior as well as the sound-evoked activity of sound-sensitive neurons. These results, together with those from channel-dead knockin worms, suggest that DES-2/DEG-3 functions as an essential component of the sound transduction channel and might do so by forming the channel pore. This reveals an unexpected ACh-independent function of nAChRs in mechanosensation.

DISCUSSION

Among the six primary sensory modalities, hearing is unique in that it is found only in vertebrates and some arthropods. This has led to the view that all non-arthropod invertebrate species are insensitive to sound (Budelmann, 1992; Faure et al., 2009; Webster, 1992). On the other hand, given that the primary function of hearing is believed to detect predators and prey (Gans, 1992; Webster, 1992), the ability to sense sound would be expected to have evolved more widely across animal phyla. However, the search for such sound-sensitive animals has not been very successful (Budelmann, 1992; Faure et al., 2009; Webster, 1992). Here, we show that the nematode *C. elegans*, an animal that lacks ear organs, senses airborne sound. Interestingly, worms can locate sound sources and engage in aversive phonotaxis behavior to avoid sound sources. Thus, the ability to sense airborne sound is not restricted to vertebrates and arthropods. Our results also show that animals without morphologically distinct ear organs may not be presumed to be insensitive to sound.

C. elegans live primarily in composts and rotting materials above ground (Félix and Braendle, 2010) and are vulnerable to their predators, such as insects and centipedes (Kiontke and Fitch, 2013). In addition, as worms feed on and inhabit decaying materials such as rotting fruits and insect host cadavers (for parasitic nematodes), they may fall prey to omnivores and scavenger insects (e.g., beetles and ants) indirectly (Ulug et al., 2014). Many such predatory animals generate loud audible sounds through stridulation (e.g., insects and centipedes) and/or wing beating (e.g., insects) (Bennet-Clark, 1975; Masters, 1980), as well as produce loud rustling sounds during foraging (e.g., insects and centipedes) (Goerlitz and Siemers, 2007; Siemers and Güttinger, 2006). The ability to detect sound sources and engage in aversive phonotaxis behavior might potentially help worms to evade such predatory animals. Nevertheless, whether this is ecologically relevant in the wild remains to be tested.

One striking observation is that sound actively vibrates worm skin, which is essential for the activation of phonotaxis behavior.

mutant worms was similar to that in wild-type (E), mutant worms responded more robustly to sound by executing more head swings (reversal duration) during reversal than wild-type worms (F). ***$p < 0.0001$ (ANOVA with Bonferroni test). $n \geq 10$.

(G–I) Knockin worms carrying mutations that enhance the channel function of DES-2/DEG-3 show enhanced sound-evoked calcium responses in FLP neurons. (G) Average traces. (H) Bar graph showing the amplitude of calcium responses. (I) Bar graph showing the deactivation kinetics of calcium responses. *$p < 0.05$; **$p < 0.005$ (t test). $n \geq 10$.

All error bars denote SEM. See also Figures S5 and S6.

In this case, worm skin functions as a sound pressure-to-displacement transducer in a manner similar to vertebrate/insect tympanum (eardrum). Notably, the displacement values of sound-evoked vibrations in worm skin are similar to those reported for human eardrum measured at similar frequencies (Goode et al., 1993, 1996). Although the exact mechanisms are unclear, the fact that worm cuticle and mammalian eardrum both have collagen as a core component might contribute to this phenomenon (Cohen and Sundaram, 2020; Stenfeldt et al., 2006). Interestingly, the sound-sensitive neurons FLP and PVD are closely associated with the skin, with their soma and sensory dendrites attached to the epidermis (Albeg et al., 2011; Inberg et al., 2019; Sundararajan et al., 2019). In addition, their sensory dendrites form an elaborate net-like structure that tiles and envelopes the entire body wall of the worm (Albeg et al., 2011; Inberg et al., 2019; Sundararajan et al., 2019). These morphological features make FLP and PVD neurons well positioned for detecting sound-evoked vibrations in the skin. Moreover, the receptive field of FLP and PVD neurons covers distinct areas of the worm body, with the dendrites of FLP enveloping the head and those of PVD occupying the body/tail (Albeg et al., 2011; Inberg et al., 2019; Sundararajan et al., 2019). As FLP and PVD are coupled to distinct downstream interneuron circuits, their activation drives reversals and forward movements, respectively (Husson et al., 2012; Li et al., 2011). These characteristics may contribute to worms' ability to locate and avoid sound sources from different directions.

Interestingly, FLP/PVD sound-sensitive neurons can also be activated by other mechanical stimuli such as noxious touch and body stretch (Albeg et al., 2011; Li et al., 2011; Tao et al., 2019). However, noxious touch represents a much more intense stimulus than sound waves (Cho et al., 2017; Tao et al., 2019), and body stretch only weakly activates these sound-sensitive neurons (Tao et al., 2019). For example, for noxious touch stimuli, a >20 μm cuticle displacement is required to activate PVD neurons (Cho et al., 2017), whereas for sound waves, a cuticle displacement in the nanometer range is sufficient to activate the same PVD neurons (Figures 2D and 3E). As such, airborne sound likely represents the most effective mechanical stimulus that activates FLP/PVD neurons. Perhaps these sound-sensitive neurons are geared to high-frequency mechanical stimuli such as sound waves, which might underlie their relatively low sensitivity to other mechanical stimuli such as touch and stretch. Remarkably, by comparing their activation thresholds, worms might potentially be as sensitive or even more sensitive to airborne sound than many vertebrate animals such as salamanders, lungfish, and some turtles (Christensen-Dalsgaard et al., 2012; Christensen et al., 2015a, 2015b). Worms also respond to a wider range of sound frequencies than these vertebrate animals (Christensen-Dalsgaard et al., 2012; Christensen et al., 2015a, 2015b).

One popular definition of hearing was proposed by Glen Wever as "the response of an animal to sound vibrations by means of a special organ for which such vibrations are the most effective stimulus" (Wever, 1974). In light of Wever's view, worm skin together with FLP/PVD sound-sensitive neurons would form a special sensory "organ" for sound detection, with sound being the most effective stimulus. We thus propose that this sound-sensing "organ," though morphologically distinct from vertebrate and insect ears, possesses functional features similar to its vertebrate and insect counterparts.

Despite notable similarities, auditory sensation in *C. elegans*, insects, and vertebrates manifests clear distinctions. One of the most striking such distinctions probably lies at the molecular level. As a comparison, all animal species use opsins to detect light (Suga et al., 2008; Terakita, 2005), with the exception of worms, which sense light through LITE-1, a non-opsin type of photoreceptor (Ghosh et al., 2021; Gong et al., 2016). In contrast, auditory sensation in vertebrates, insects and *C. elegans* appear to rely on distinct classes of mechanotransduction channels. Specifically, vertebrates depend on TMC channels to transduce sound signals (Jia et al., 2020; Pan et al., 2013), while insects (e.g., *Drosophila*) require TRP family channels for sound sensing (Göpfert and Hennig, 2016). In *C. elegans*, we found that sound-sensitive FLP/PVD neurons do not require TMC or TRP family channels, but instead depend on a nAChR channel (DES-2/DEG-3). Surprisingly, this role of DES-2/DEG-3 is independent of its function as an ACh receptor, indicating that it plays a more direct role in the process. Indeed, further analysis shows that this nAChR functions as an essential component of the sound transduction channel and might do so by forming the channel pore. We thus propose that DES-2/DEG-3 might function as pore-forming subunits of a mechanotransduction channel complex/apparatus that transduces sound stimuli in sound-sensitive neurons. This role of DES-2/DEG-3 would be similar to that of the ENaC/DEG channel subunits MEC-4/MEC-10 in the mechanotransduction channel complex/apparatus that transduces touch stimuli in *C. elegans* touch receptor neurons (Bounoutas and Chalfie, 2007). nAChRs are best known to function as ACh receptors that mediate nicotine dependence in the brain and muscle contractions at the neuromuscular junctions. Although nAChRs have been implicated in mechanosensation in worms and mammalian cells, such a role is indirect, as it depends on ACh (Cohen et al., 2014; Pan et al., 2012). Our results unveil an unexpected ACh-independent function of nAChRs in mechanosensation.

Concluding remarks

In summary, we show that despite the lack of ears, the nematode *C. elegans* senses airborne sound. Worms detect sound through their skin, which acts in a manner similar to the eardrum in vertebrate and insect ears. At the molecular level, worms transduce sound signals through a mechanotransduction channel apparatus that is distinct from that used by vertebrates and insects. Apparently, auditory sensation in *C. elegans*, insects, and vertebrates bears both similarities and distinctions. We thus conclude that the ability to sense airborne sound is not restricted to vertebrates and arthropods as believed previously. This supports the notion that auditory sensation might have evolved multiple times independently across animal phyla, suggesting convergent evolution. This stands in sharp contrast to the evolution of vision, which, as proposed by Charles Darwin, occurred relatively early and probably only once with a monophyletic origin (Gehring, 2014). Our studies also raise the intriguing possibility that other earless invertebrates, particularly those with soft bodies like *C. elegans*, such as terrestrial mollusks, annelids, and flatworms, might also possess the ability to sense airborne sound.

STAR★METHODS

Detailed methods are provided in the online version of this paper and include the following:

- KEY RESOURCES TABLE
- RESOURCE AVAILABILITY
  - Lead contact
  - Materials availability
  - Data and code availability
- EXPERIMENTAL MODEL AND SUBJECT DETAILS
  - Animals
  - Cell lines
- METHOD DETAILS
  - Molecular biology and genetics
  - Genetic screen and genome editing
  - Sound generation, delivery and measurement
  - Behavioral assays
  - Laser Doppler vibrometry
  - Calcium imaging
  - Electrophysiology
  - Confocal microscopy
- QUANTIFICATION AND STATISTICAL ANALYSIS

SUPPLEMENTAL INFORMATION

Supplemental information can be found online at https://doi.org/10.1016/j.neuron.2021.08.035.

ACKNOWLEDGMENTS

We thank Bing Ye for critically reading the manuscript; Teng Yu, Deepak Dileepkumar, and Kalynn Bird for technical assistance; and Jonathan Ronan for graphic design and video editing. Some strains were obtained from the Caenorhabditis Genetics Center (CGC). Some figure graphics were created using Biorender.com. A.J.I. and E.A.R. received support from an NIH T32 training grant. A.J.I. received support from an NIH F32 grant. This work was first supported by an R35 grant from the National Institute of General Medical Sciences (NIGMS) (to X.Z.S.X.) and then jointly by an R01 grant from the National Institute on Deafness and Other Communication Disorders (NIDCD) (to X.Z.S.X.).

AUTHOR CONTRIBUTIONS

A.J.I. initiated the project. C.W. and A.J.I. performed most of the experiments and analyzed the data. E.A.R. performed laser Doppler vibrometry and analyzed the data with assistance from A.E.H. and K.G. C.W. and Y.G. performed EMS screens. X.L. performed electrophysiological recordings. X.Z. assisted C.W. and Y.G. in analyzing whole-genome sequencing data. R.K.D. provided technical assistance to A.J.I. R.K.D. and J.L. participated in the early phase of the work. E.A.R. and C.W. prepared the figures. X.Z.S.X. supervised the project and wrote the paper with assistance from E.A.R., C.W., A.J.I., J.L., and all other authors.

DECLARATION OF INTERESTS

The authors declare no competing interests.

Received: April 27, 2021
Revised: July 21, 2021
Accepted: August 27, 2021
Published: September 22, 2021

REFERENCES

Ache, B.W., and Young, J.M. (2005). Olfaction: diverse species, conserved principles. Neuron *48*, 417–430.

Albeg, A., Smith, C.J., Chatzigeorgiou, M., Feitelson, D.G., Hall, D.H., Schafer, W.R., Miller, D.M., 3rd, and Treinin, M. (2011). C. elegans multi-dendritic sensory neurons: morphology and function. Mol. Cell. Neurosci. *46*, 308–317.

Alfonso, A., Grundahl, K., Duerr, J.S., Han, H.P., and Rand, J.B. (1993). The Caenorhabditis elegans unc-17 gene: a putative vesicular acetylcholine transporter. Science *261*, 617–619.

Alfonso, A., Grundahl, K., McManus, J.R., and Rand, J.B. (1994). Cloning and characterization of the choline acetyltransferase structural gene (cha-1) from C. elegans. J. Neurosci. *14*, 2290–2300.

Arribere, J.A., Bell, R.T., Fu, B.X., Artiles, K.L., Hartman, P.S., and Fire, A.Z. (2014). Efficient marker-free recovery of custom genetic modifications with CRISPR/Cas9 in Caenorhabditis elegans. Genetics *198*, 837–846.

Bargmann, C.I., and Horvitz, H.R. (1991). Chemosensory neurons with overlapping functions direct chemotaxis to multiple chemicals in C. elegans. Neuron *7*, 729–742.

Bargmann, C.I., Hartwieg, E., and Horvitz, H.R. (1993). Odorant-selective genes and neurons mediate olfaction in C. elegans. Cell *74*, 515–527.

Bennet-Clark, H.C. (1975). Sound production in insects. Sci. Prog. *62*, 263–283.

Bercher, M., Wahl, J., Vogel, B.E., Lu, C., Hedgecock, E.M., Hall, D.H., and Plenefisch, J.D. (2001). mua-3, a gene required for mechanical tissue integrity in Caenorhabditis elegans, encodes a novel transmembrane protein of epithelial attachment complexes. J. Cell Biol. *154*, 415–426.

Bounoutas, A., and Chalfie, M. (2007). Touch sensitivity in Caenorhabditis elegans. Pflugers Arch. *454*, 691–702.

Budelmann, B.U. (1992). Hearing in nonarthropod invertebrates. In The Evolutionary Biology of Hearing, D.B. Webster, R.R. Fay, and A.N. Popper, eds. (Springer-Verlag), pp. 141–155.

Chalfie, M., Sulston, J.E., White, J.G., Southgate, E., Thomson, J.N., and Brenner, S. (1985). The neural circuit for touch sensitivity in Caenorhabditis elegans. J. Neurosci. *5*, 956–964.

Cho, Y., Porto, D.A., Hwang, H., Grundy, L.J., Schafer, W.R., and Lu, H. (2017). Automated and controlled mechanical stimulation and functional imaging in vivo in C. elegans. Lab Chip *17*, 2609–2618.

Christensen, C.B., Christensen-Dalsgaard, J., and Madsen, P.T. (2015a). Hearing of the African lungfish (Protopterus annectens) suggests underwater pressure detection and rudimentary aerial hearing in early tetrapods. J. Exp. Biol. *218*, 381–387.

Christensen, C.B., Lauridsen, H., Christensen-Dalsgaard, J., Pedersen, M., and Madsen, P.T. (2015b). Better than fish on land? Hearing across metamorphosis in salamanders. Proc. Biol. Sci. *282*, 20141943.

Christensen-Dalsgaard, J., and Carr, C.E. (2008). Evolution of a sensory novelty: tympanic ears and the associated neural processing. Brain Res. Bull. *75*, 365–370.

Christensen-Dalsgaard, J., Brandt, C., Willis, K.L., Christensen, C.B., Ketten, D., Edds-Walton, P., Fay, R.R., Madsen, P.T., and Carr, C.E. (2012). Specialization for underwater hearing by the tympanic middle ear of the turtle, Trachemys scripta elegans. Proc. Biol. Sci. *279*, 2816–2824.

Cohen, J.D., and Sundaram, M.V. (2020). *C. elegans* apical extracellular matrices shape epithelia. J. Dev. Biol. *8*, E23.

Cohen, E., Chatzigeorgiou, M., Husson, S.J., Steuer-Costa, W., Gottschalk, A., Schafer, W.R., and Treinin, M. (2014). Caenorhabditis elegans nicotinic acetylcholine receptors are required for nociception. Mol. Cell. Neurosci. *59*, 85–96.

Criado, M., Svobodová, L., Mulet, J., Sala, F., and Sala, S. (2011). Substitutions of amino acids in the pore domain of homomeric α7 nicotinic receptors for analogous residues present in heteromeric receptors modify gating, rectification and binding properties. J. Neurochem. *119*, 40–49.

Dickinson, D.J., Pani, A.M., Heppert, J.K., Higgins, C.D., and Goldstein, B. (2015). Streamlined genome engineering with a self-excising drug selection cassette. Genetics *200*, 1035–1049.

Driscoll, M., and Chalfie, M. (1991). The mec-4 gene is a member of a family of Caenorhabditis elegans genes that can mutate to induce neuronal degeneration. Nature *349*, 588–593.

Eastwood, A.L., Sanzeni, A., Petzold, B.C., Park, S.J., Vergassola, M., Pruitt, B.L., and Goodman, M.B. (2015). Tissue mechanics govern the rapidly adapting and symmetrical response to touch. Proc. Natl. Acad. Sci. U S A *112*, E6955–E6963.

Edwards, S.L., Charlie, N.K., Milfort, M.C., Brown, B.S., Gravlin, C.N., Knecht, J.E., and Miller, K.G. (2008). A novel molecular solution for ultraviolet light detection in Caenorhabditis elegans. PLoS Biol. *6*, e198.

Faure, P.A., Mason, A.C., and Yack, J.E. (2009). Invertebrate ears and hearing. In Encyclopedia of the Neuroscience, L.R. Squire, ed. (Elsevier), pp. 2035–2042.

Félix, M.A., and Braendle, C. (2010). The natural history of Caenorhabditis elegans. Curr. Biol. *20*, R965–R969.

Gans, C. (1992). An overview of the evolutionary biology of hearing. In The Evolutionary Biology of Hearing, D.B. Webster, R.R. Fay, and A.N. Popper, eds. (Springer-Verlag), pp. 3–13.

Gehring, W.J. (2014). The evolution of vision. Wiley Interdiscip. Rev. Dev. Biol. *3*, 1–40.

Ghosh, D.D., Lee, D., Jin, X., Horvitz, H.R., and Nitabach, M.N. (2021). *C. elegans* discriminates colors to guide foraging. Science *371*, 1059–1063.

Goerlitz, H.R., and Siemers, B.M. (2007). Sensory ecology of prey rustling sounds: acoustical features and their classification by wild grey mouse lemurs. Funct. Ecol. *21*, 143–153.

Gong, J., Yuan, Y., Ward, A., Kang, L., Zhang, B., Wu, Z., Peng, J., Feng, Z., Liu, J., and Xu, X.Z.S. (2016). The C. elegans taste receptor homolog LITE-1 is a photoreceptor. Cell *167*, 1252–1263.e10.

Gong, J., Liu, J., Ronan, E.A., He, F., Cai, W., Fatima, M., Zhang, W., Lee, H., Li, Z., Kim, G.H., et al. (2019). A cold-sensing receptor encoded by a glutamate receptor gene. Cell *178*, 1375–1386.e11.

Goode, R.L., Ball, G., and Nishihara, S. (1993). Measurement of umbo vibration in human subjects–method and possible clinical applications. Am. J. Otol. *14*, 247–251.

Goode, R.L., Ball, G., Nishihara, S., and Nakamura, K. (1996). Laser Doppler vibrometer (LDV)—a new clinical tool for the otologist. Am. J. Otol. *17*, 813–822.

Goodman, M.B., Ernstrom, G.G., Chelur, D.S., O'Hagan, R., Yao, C.A., and Chalfie, M. (2002). MEC-2 regulates C. elegans DEG/ENaC channels needed for mechanosensation. Nature *415*, 1039–1042.

Göpfert, M.C., and Hennig, R.M. (2016). Hearing in insects. Annu. Rev. Entomol. *61*, 257–276.

Holbrook, R.I., and Mortimer, B. (2018). Vibration sensitivity found in *Caenorhabditis elegans*. J. Exp. Biol. *221*, jeb178947.

Husson, S.J., Costa, W.S., Wabnig, S., Stirman, J.N., Watson, J.D., Spencer, W.C., Akerboom, J., Looger, L.L., Treinin, M., Miller, D.M., 3rd, et al. (2012). Optogenetic analysis of a nociceptor neuron and network reveals ion channels acting downstream of primary sensors. Curr. Biol. *22*, 743–752.

Iliff, A.J., and Xu, X.Z.S. (2020). *C. elegans:* a sensible model for sensory biology. J. Neurogenet. *34*, 347–350.

Inberg, S., Meledin, A., Kravtsov, V., Iosilevskii, Y., Oren-Suissa, M., and Podbilewicz, B. (2019). Lessons from worm dendritic patterning. Annu. Rev. Neurosci. *42*, 365–383.

Jia, Y., Zhao, Y., Kusakizako, T., Wang, Y., Pan, C., Zhang, Y., Nureki, O., Hattori, M., and Yan, Z. (2020). TMC1 and TMC2 proteins are pore-forming subunits of mechanosensitive ion channels. Neuron *105*, 310–321.e3.

Katsuki, T., and Greenspan, R.J. (2013). Jellyfish nervous systems. Curr. Biol. *23*, R592–R594.

Kiontke, K., and Fitch, D.H. (2013). Nematodes. Curr. Biol. *23*, R862–R864.

Labarca, C., Nowak, M.W., Zhang, H., Tang, L., Deshpande, P., and Lester, H.A. (1995). Channel gating governed symmetrically by conserved leucine residues in the M2 domain of nicotinic receptors. Nature *376*, 514–516.

Li, W., Feng, Z., Sternberg, P.W., and Xu, X.Z.S. (2006). A C. elegans stretch receptor neuron revealed by a mechanosensitive TRP channel homologue. Nature *440*, 684–687.

Li, W., Kang, L., Piggott, B.J., Feng, Z., and Xu, X.Z.S. (2011). The neural circuits and sensory channels mediating harsh touch sensation in Caenorhabditis elegans. Nat. Commun. *2*, 315.

Masters, W.M. (1980). Insect disturbance stridulation—characterization of airborne and vibrational components of the sound. J. Comp. Physiol. *135*, 259–268.

Mill, P.J. (1976). Structure and Function of Proprioceptors in the Invertebrates (Chapman & Hall).

Pan, N.C., Ma, J.J., and Peng, H.B. (2012). Mechanosensitivity of nicotinic receptors. Pflugers Arch. *464*, 193–203.

Pan, B., Géléoc, G.S., Asai, Y., Horwitz, G.C., Kurima, K., Ishikawa, K., Kawashima, Y., Griffith, A.J., and Holt, J.R. (2013). TMC1 and TMC2 are components of the mechanotransduction channel in hair cells of the mammalian inner ear. Neuron *79*, 504–515.

Piggott, B.J., Liu, J., Feng, Z., Wescott, S.A., and Xu, X.Z.S. (2011). The neural circuits and synaptic mechanisms underlying motor initiation in C. elegans. Cell *147*, 922–933.

Pokala, N., Liu, Q., Gordus, A., and Bargmann, C.I. (2014). Inducible and titratable silencing of Caenorhabditis elegans neurons in vivo with histamine-gated chloride channels. Proc. Natl. Acad. Sci. U S A *111*, 2770–2775.

Prescott, T.J., and Dürr, V. (2015). The world of touch. Scholarpedia *10*, 32688.

Rabinowitz, P.M. (2000). Noise-induced hearing loss. Am. Fam. Physician *61*, 2749–2756, 2759–2760.

Revah, F., Bertrand, D., Galzi, J.L., Devillers-Thiéry, A., Mulle, C., Hussy, N., Bertrand, S., Ballivet, M., and Changeux, J.P. (1991). Mutations in the channel domain alter desensitization of a neuronal nicotinic receptor. Nature *353*, 846–849.

Richmond, J.E., Davis, W.S., and Jorgensen, E.M. (1999). UNC-13 is required for synaptic vesicle fusion in C. elegans. Nat. Neurosci. *2*, 959–964.

Russell, J., Vidal-Gadea, A.G., Makay, A., Lanam, C., and Pierce-Shimomura, J.T. (2014). Humidity sensation requires both mechanosensory and thermosensory pathways in Caenorhabditis elegans. Proc. Natl. Acad. Sci. U S A *111*, 8269–8274.

Schellart, N.A.M., and Popper, A.N. (1992). Functional aspects of the evolution of the auditory system of actinopterygian fish. In The Evolutionary Biology of Hearing, D.B. Webster, R.R. Fay, and A.N. Popper, eds. (Springer-Verlag), pp. 295–322.

Siemers, B.M., and Güttinger, R. (2006). Prey conspicuousness can explain apparent prey selectivity. Curr. Biol. *16*, R157–R159.

Speese, S., Petrie, M., Schuske, K., Ailion, M., Ann, K., Iwasaki, K., Jorgensen, E.M., and Martin, T.F. (2007). UNC-31 (CAPS) is required for dense-core vesicle but not synaptic vesicle exocytosis in Caenorhabditis elegans. J. Neurosci. *27*, 6150–6162.

Stenfeldt, K., Johansson, C., and Hellström, S. (2006). The collagen structure of the tympanic membrane: collagen types I, II, and III in the healthy tympanic membrane, during healing of a perforation, and during infection. Arch. Otolaryngol. Head Neck Surg. *132*, 293–298.

Suga, H., Schmid, V., and Gehring, W.J. (2008). Evolution and functional diversity of jellyfish opsins. Curr. Biol. *18*, 51–55.

Sundararajan, L., Stern, J., and Miller, D.M., 3rd (2019). Mechanisms that regulate morphogenesis of a highly branched neuron in C. elegans. Dev. Biol. *451*, 53–67.

Tao, L., Porto, D., Li, Z., Fechner, S., Lee, S.A., Goodman, M.B., Xu, X.Z.S., Lu, H., and Shen, K. (2019). Parallel Processing of Two Mechanosensory Modalities by a Single Neuron in C. elegans. Dev. Cell *51*, 617–631.e3.

Terakita, A. (2005). The opsins. Genome Biol. *6*, 213.

Treinin, M., Gillo, B., Liebman, L., and Chalfie, M. (1998). Two functionally dependent acetylcholine subunits are encoded in a single Caenorhabditis elegans operon. Proc. Natl. Acad. Sci. U S A *95*, 15492–15495.

Tsalik, E.L., Niacaris, T., Wenick, A.S., Pau, K., Avery, L., and Hobert, O. (2003). LIM homeobox gene-dependent expression of biogenic amine receptors in restricted regions of the C. elegans nervous system. Dev. Biol. *263*, 81–102.

Ulug, D., Hazir, S., Kaya, H.K., and Lewis, E. (2014). Natural enemies of natural enemies: the potential top-down impact of predators on entomopathogenic nematode populations. Ecol. Entomol. *39*, 462–469.

Wang, X., Li, G., Liu, J., Liu, J., and Xu, X.Z. (2016). TMC-1 mediates alkaline sensation in C. elegans through nociceptive neurons. Neuron *91*, 146–154.

Wang, X., Li, T., Hu, J., Feng, Z., Zhong, R., Nie, W., Yang, X., and Zou, Y. (2021). *In vivo* imaging of a PVD neuron in *Caenorhabditis elegans*. STAR Protoc *2*, 100309.

Ward, S. (1973). Chemotaxis by the nematode Caenorhabditis elegans: identification of attractants and analysis of the response by use of mutants. Proc. Natl. Acad. Sci. U S A *70*, 817–821.

Ward, A., Liu, J., Feng, Z., and Xu, X.Z. (2008). Light-sensitive neurons and channels mediate phototaxis in C. elegans. Nat. Neurosci. *11*, 916–922.

Way, J.C., and Chalfie, M. (1989). The mec-3 gene of Caenorhabditis elegans requires its own product for maintained expression and is expressed in three neuronal cell types. Genes Dev. *3* (12A), 1823–1833.

Webster, D.B. (1992). Epilogue to the conference on the evolutionary biology of hearing. In The Evolutionary Biology of Hearing, D.B. Webster, R.R. Fay, and A.N. Popper, eds. (Springer-Verlag), pp. 787–793.

Wever, E.G. (1974). The evolution of vertebrate hearing. In Handbook of Sensory Physiology, W.D. Keidel and W.D. Neff, eds. (Springer-Verlag), pp. 423–454.

Wicher, D. (2012). Functional and evolutionary aspects of chemoreceptors. Front. Cell. Neurosci. *6*, 48.

Wicks, S.R., and Rankin, C.H. (1995). Integration of mechanosensory stimuli in Caenorhabditis elegans. J. Neurosci. *15*, 2434–2444.

STAR★METHODS

KEY RESOURCES TABLE

REAGENT or RESOURCE	SOURCE	IDENTIFIER
Bacterial and virus strains		
E. coli: OP50	Caenorhabditis Genetics Center	OP50
Experimental models: Cell lines		
HEK293T	ATCC	ACS-4500
Experimental models: Organisms/strains		
Wild type: N2.	Caenorhabditis Genetics Center	WB strain: N2.
mec-4(e1611).	Caenorhabditis Genetics Center	TQ528
bli-1(e769).	Caenorhabditis Genetics Center	TQ10560
bli-2(e768).	Caenorhabditis Genetics Center	TQ10419
bli-6(sc16).	Caenorhabditis Genetics Center	TQ10421
mec-3(e1338).	Caenorhabditis Genetics Center	TQ526
xuEx3483[Psto-5::dHisCl::YFP].	This paper	TQ10245
xuEx3484[Pser-2(prom3)::dHisCl::YFP].	This paper	TQ10246
xuEx2708[Psto-5::GCaMP6(f)+Psto-5::mCherry2].	This paper	TQ9905
xuIs531[Pser-2(prom3)::GCaMP6(f) + Pser-2(prom3)::mCherry].	This paper	TQ9910
unc-13(e51); xuEx2708[Psto-5::GCaMP6(f)+Psto-5::mCherry2].	This paper	TQ9193
unc-31(e169); xuEx2708[Psto-5::GCaMP6(f)+Psto-5::mCherry2].	This paper	TQ9197
unc-13(e51); xuIs531[Pser-2(prom3)::GCaMP6(f) + Pser-2(prom3)::mCherry].	This paper	TQ9372
unc-31(e169); xuIs542[Pser-2(prom3)::GCaMP6(f) + Pser-2(prom3)::mCherry].	This paper	TQ10558
pezo-1(xu112)	This paper	TQ4342
trp-4(sy695).	(Li et al., 2006)	TQ109
tmc-1(ok1859) tmc-2(ok1302).	This paper	TQ3369
osm-9(ky10).	Caenorhabditis Genetics Center	TQ472
del-1(ok150); mec-10(tm1552); unc-8(tm2071).	(Tao et al., 2019)	TQ10553
degt-1(ok3307).	Caenorhabditis Genetics Center	TQ9155
pezo-1(xu112); xuEx2708[Psto-5::GCaMP6(f)+Psto-5::mCherry2].	This paper	TQ9866
trp-4(sy695); xuEx2708[Psto-5::GCaMP6(f)+Psto-5::mCherry2].	This paper	TQ10429
tmc-1(ok1859) tmc-2(ok1302); xuEx2708[Psto-5::GCaMP6(f)+Psto-5::mCherry2].	This paper	TQ10425
osm-9(ky10); xuEx2708[Psto-5::GCaMP6(f)+Psto-5::mCherry2].	This paper	TQ10475
del-1(ok150); mec-10(tm1552); unc-8(tm2071); xuEx2708[Psto-5::GCaMP6(f)+Psto-5::mCherry2].	This paper	TQ9590
degt-1(ok3307); xuEx2708[Psto-5::GCaMP6(f)+Psto-5::mCherry2].	This paper	TQ9199
des-2(xu461).	This paper	TQ7712
deg-3(xu462).	This paper	TQ7713
des-2 deg-3(xu482).	This paper	TQ7723
des-2 deg-3(xu482); xuEx3317[Psto-5::des-2::sl2::CFP+Psto-5::deg-3::sl2::CFP].	This paper	TQ9922
des-2 deg-3(xu482); xuEx2708[Psto-5::GCaMP6(f) + Psto-5::mCherry2].	This paper	TQ8026

(*Continued on next page*)

Continued

REAGENT or RESOURCE	SOURCE	IDENTIFIER
des2 deg3(xu482); xuEx2708[Psto-5::GCaMP6(f)+Psto 5::mCherry2]; xuEx3317[Psto-5::des-2::sl2::CFP+Psto-5::deg-3::sl2::CFP].	This paper	TQ9909
des-2(xu644[des-2::mNeoGreen::flag])	This paper	TQ10430
deg-3(xu676[deg-3::mNeoGreen::flag])	This paper	TQ9812
unc-17(e245); xuEx2708[Psto-5::GCaMP6(f)+Psto-5::mCherry2].	This paper	TQ9597
cha-1(p1152); xuEx2708[Psto-5::GCaMP6(f)+Psto-5::mCherry2].	This paper	TQ9596
des-2 deg-3(xu482); xuEx3355[Psto-5::des2(S292R)::sl2::CFP+Psto-5::deg3(S320R)::sl2::CFP].	This paper	TQ9973
des-2 deg-3(xu482); xuEx3378[Psto-5::des2(G277K)::sl2::CFP+Psto-5::deg3(G305K)::sl2::CFP].	This paper	TQ9975
des-2(S292R)::mNeonGreen::flag.	This paper	TQ10438
des-2(G277K)::mNeonGreen::flag.	This paper	TQ10433
des-2(G277K)::mNeonGreen; xuEx2708[Psto-5::GCaMP6(f)+Psto-5::mCherry2].	This paper	TQ10338
des-2(S292R)::mNeonGreen; xuEx2708[Psto-5::GCaMP6(f)+Psto-5::mCherry2].	This paper	TQ10339
des-2::mNeonGreen; xuEx2708[Psto-5::GCaMP6(f)+Psto-5::mCherry2].	This paper	TQ10337
des-2(L282S)::mNeonGreen; deg-3(L310S).	This paper	TQ10434
des-2(L282S)::mNeonGreen deg-3(L310S); xuEx2708[Psto-5::GCaMP6(f)+ Psto-5::mCherry2].	This paper	TQ10340
des-2 deg-3(xu482); xuIs531[Pser-2(prom3)::GCaMP6(f) + Pser-2(prom3)::mCherry].	This paper	TQ8918
deg-3::mNeonGreen; xuEx2708[Psto-5::GCaMP6(f)+Psto-5::mCherry2].	This paper	TQ10552
Oligonucleotides		
Primer: for *des-2* mNeongreen knockin: guide RNA fwd: CAAGCTGGTGTTG AATATGG GTTTTAGAGCTAGAAATAGC	This paper	N/A
Primer: for *des-2* mNeongreen knockin: 5′ arm fwd: acgttgtaaaacgacggccagtcgccggcaatcta ctagaacaatccaac	This paper	N/A
Primer: for *des-2* mNeongreen knockin: 5′ arm rev: CATCGATGCTCCTGAGGCTCCCGATGCTCCTCC TCCGTACTCTACTCCTGCTTG ATGCCAGTGAA TGAAACCAATG	This paper	N/A
Primer: for *des-2* mNeongreen knockin: 3′ arm fwd: CGTGATTACAAGGATGACGATGACAAGAGA TGAacattctcattttcatc	This paper	N/A
Primer: for *des-2* mNeongreen knockin: 3′ arm rev: ggaaacagctatgaccatgttatcgatttc gagtctgggaatactcaccg	This paper	N/A
Primer: for *deg-3* mNeongreen knockin: guide RNA fwd: CACAATACAGTTATGACCACCGTTTTAGAGCTAGAAATAGC	This paper	N/A
Primer: for *deg-3* mNeongreen knockin: 5′ arm fwd: acgttgtaaaacgacggccagtcgccggcaaatttcagGTCCACATTGCG	This paper	N/A

(*Continued on next page*)

Continued

REAGENT or RESOURCE	SOURCE	IDENTIFIER
Primer: for *deg-3* mNeongreen knockin: 5′ arm rev: CATCGATGCTCCTGAGGCTCCCGATGCTCC GACATTAAAGAATCGGTCATCT	This paper	N/A
Primer: for *deg-3* mNeongreen knockin: 3′ arm fwd: CGTGATTACAAGGATGACGATGACAAGAGA TAAaacttatctcttttttcc	This paper	N/A
Primer: for *deg-3* mNeongreen knockin: 3′ arm rev: ggaaacagctatgaccatgttatcgatttcctgaactaacaatacggaag	This paper	N/A
Recombinant DNA		
Plasmid: pcDNA3.0::Flag::deg-3(cDNA)	This paper	pSX2507
Plasmid: pcDNA3.0::Flag::des-2(cDNA)	This paper	pSX3236
Plasmid: pBS77::Psto-5::des-2(c)::sl2::CFP	This paper	pSX2782
Plasmid: Psto-5::deg-3(c)::sl2::CFP	This paper	pSX2829
Plasmid: pcDNA3.0::flag::des-2(L282S)	This paper	pSX2905
Plasmid: pcDNA3.0::flag::des-2(G277K)	This paper	pSX2908
Plasmid: pcDNA3.0::flag::des-2(S292R)	This paper	pSX2910
Plasmid: pcDNA3.0::flag::deg-3(L310S)	This paper	pSX2914
Plasmid: pcDNA3.0::flag::deg-3(G305K)	This paper	pSX2917
Plasmid: pcDNA3.0::flag::deg-3(S320R)	This paper	pSX2919
Plasmid: Psto-5::des-2(G277K)::sl2::CFP	This paper	pSX2954
Plasmid: Psto-5::deg-3(G305K)::sl2::CFP	This paper	pSX2955
Plasmid: Psto-5::des-2(S292R)::sl2::CFP	This paper	pSX2958
Plasmid: Psto-5::deg-3(S320R)::sl2::CFP	This paper	pSX2959
Plasmid: Psto-5::dHicCL::sl2::YFP	This paper	pSX3116
Plasmid: Pser-2(3)::dHisCl::sl2::YFP	This paper	pSX3235
Plasmid: pBS77::pSto-5::GCaMP6f	This paper	pSX1788
Plasmid: pBS77:: Psto-5::SL2::mCherry2	This paper	pSX1784
Software and algorithms		
GraphPad	GraphPad Software, Inc	N/A
Multi-Instrument Standard 3.9 audio software	Virtins Technology	https://www.virtins.com/multi-instrument.shtml
MATLAB	MathWorks	R2017b
APx500 v6.0 Audio Measurement Software	Audio Precision	https://www.ap.com/download/apx500-measurement-software-18/
Other		
Multi-field speakers	Tucker-Davis Technologies (TDT)	MF-1
Audio amplifier	Parasound	Zamp v.3
Function Arbitrary Waveform Generator	Brüel & Kjær	Type 4052
1/8 inch microphone	Brüel & Kjær	Type 4183
Microphone preamp	Brüel & Kjær	Type 2619
Microphone power supply	Brüel & Kjær	Type 2804
Analog electret condenser omnidirectional microphone	Knowles	FG-23329-P07
USB Audio Interface	Focusrite	SCARLETT-SOLO-3G
Ultra-Low Distortion Oscillator	Krohn-Hite	Model 4400A
Spectrum analyzer	Stanford Research Systems	Model SR760
6 mm omni-directional electret condenser USB microphone	Virtins	VT RTA-168B
1/8 inch CCP Pressure Standard Microphone Set	GRAS	46DE
Sound level calibrator	REED Instruments	R8090
Acoustic audio analyzer/amplifier	Audio Precision	APx517B

RESOURCE AVAILABILITY

Lead contact

Further information and requests for resources and reagents should be directed to and will be fulfilled by the lead contact X.Z. Shawn Xu (shawnxu@umich.edu).

Materials availability

This study has generated plasmids and *C. elegans* strains, which are listed in the Key resources table. These reagents will be made available upon request.

Data and code availability

All data reported in this paper will be shared by the lead contact upon request.

This paper does not report original code.

Any additional information required to reanalyze the data reported in this study is available from the lead contact upon request.

EXPERIMENTAL MODEL AND SUBJECT DETAILS

Animals

C. elegans strains were cultured at 20°C on standard nematode growth medium (NGM) plates seeded with OP50 bacteria. In general, day 1 adult hermaphrodites were used for experiments unless specified otherwise. Please see below in Methods details for further details. The specific genotypes of the strains used this study can be found in the Key resources table. Transgenic lines were generated by injecting plasmid DNA directly into the gonad of hermaphrodite worms. Mutant strains and integrated transgenic strains were outcrossed at least four times before use.

Cell lines

HEK293T cells were cultured in DMEM medium containing 10% fetal bovine serum (heat inactivated) in a 37°C incubator containing 5% CO2. This cell line was obtained from the ATCC. See Key resources table for details.

METHOD DETAILS

Molecular biology and genetics

For the experiments using transgenes, at least two independent transgenic lines were examined to confirm findings. *des-2* and *deg-3* cDNA were cloned by RT-PCR from total RNA isolated from WT (N2) worms. Transgene expression was verified by expression of a fluorescent marker (CFP, YFP or mCherry), which was driven by SL2 from the same transcript.

Genetic screen and genome editing

EMS was used to mutagenize worms carrying a transgene expressing GCaMP6(f) and mCherry in FLP neurons, which enables real-time visual detection of changes in GCaMP fluorescence in response to sound (2 s, 1 kHz at 80 dB SPL) using a fluorescent stereomicroscope under a 10x objective (Zeiss Discovery V8 with M2Bio). ~2000 F1 parents were plated on individually seeded NGM plates as L4 for ~12 hours prior to removal, and the offspring on each individual plate were tested (~20,000 F2). Those candidates that failed to exhibit increased fluorescence in FLP in response to sound were recovered and outcrossed to the parental strain at least five times, and both parental and candidate strains underwent whole-genome sequencing (WGS). Sequencing results were analyzed as described previously (Gong et al., 2019). By comparing the WGS data between parental and mutant strains, we obtained density maps for each candidate and mapped the mutations in three candidate strains. Molecular lesion: *xu119* carries a G259E mutation in *des-2*; *xu126* carries a nonsense mutation (W396Stop) in *des-2*; *xu121* carries a mutation in the 5′UTR of *deg-3*, and complementation tests showed that *xu121* is an allele for *deg-3*.

des-2(xu461), deg-3(xu462), and *des-2 deg-3(xu482)* are deletion mutants generated by CRISPR/Cas9-based genome editing using standard protocol as described previously (Arribere et al., 2014). No repair template was included to facilitate isolation of deletion alleles. *des-2::mNG* and *deg-3::mNG* knockin alleles were generated using standard protocol as described (Dickinson et al., 2015). The mNG::3xFLAG tag was inserted at the C-terminal end of *des-2* and *deg-3*. To generate *des-2(G277K)::mNG, des-2(S292R)::mNG,* and *des-2(L282S)::mNG deg-3(L310S)* knockin strains, the genome editing was performed in *des-2::mNG* background using standard protocol (Arribere et al., 2014). In the case of *des-2(L282S)::mNG deg-3(L310S)* knockin strain, the two point mutants were introduced sequentially. All knockout and knockin strains were outcrossed at least four times prior to use.

Sound generation, delivery and measurement

Sinusoidal tones were generated by a computer sound card using Multi-Instrument (MI) audio software (Virtins Technology). The signal from the computer was amplified (Parasound Zamp v.3) and generated by a multi-field magnetic speaker (Tucker-Davis Technologies MF-1) with the internal parabolic cone attached. The computer output (via a 3.5mm stereo audio jack) was connected to

the + and – terminals on a single channel of the amplifier. The amplifier is connected to the speaker via an RCA cable. The speaker tip was connected to a shortened pipette tip via a short length of $^{1}/_{8}$ '' PVC tubing (see Figure 1A). To protect the speaker, the amplifier gain was fixed to produce a maximum output of 10 V peak voltage at 1 kHz. In some cases, sine waves were generated by a function generator (Brüel & Kjær type 4052) connected directly to the speaker via BNC to RCA cable.

The speaker is mounted to a manual micromanipulator arm (Narishige NMN-21). An 8-32 threaded rod attached to the back of the speaker is clamped to the manipulator and positioned 30 degrees downward. The manipulator and speaker are mounted to a block to bring it up to the microscope stage level and stabilize the entire setup.

The acoustic properties of the generated sound fields emanating from the output port were determined with a small diameter analog electret condenser omnidirectional microphone (1 mm inner diameter; Knowles, FG-23329-P07) in combination with MI audio software and an external sound card (Focusrite Scarlett Solo 2x2 USB Audio Interface) connected to the computer. This miniature microphone (mini-microphone) was powered by a custom power supply (Figure S7), and connected to the external sound card via a BNC to ¼'' stereo jack adaptor. The external sound card was connected to the computer via a USB connection. Sound pressure level (SPL), total harmonic distortion, and audio spectra were collected periodically throughout the duration of the presented experiments.

Initial calibration of the mini-microphone was performed by Kresge Hearing Research Institute sound engineers against a 1/8 inch microphone (Brüel & Kjær type 4138; type 2619 preamp, and type 2804 power supply) using a sound source (Krohn-Hite model 4400A Ultra-Low Distortion Oscillator) and spectrum analyzer (Stanford Research Systems Model SR760). The calibration parameters were input in MI audio software following the developer's instructions. Subsequently, calibration parameters were routinely verified using a sound level calibrator standard (1 kHz 94 dB SPL; REED Instruments #R8090). We also verified the acoustic properties of the generated sounds using two additional microphone systems: (1) 6 mm omni-directional electret condenser USB microphone (Virtins VT RTA-168B) with the Multi-Instrument audio software; (2) 1/8'' CCP Pressure Standard Microphone Set (GRAS 46DE) with APx517B amplifier (Audio Precision) and APx500 v6.0 Audio Measurement Software (Audio Precision). Both methods gave rise to the same measurement values. We recommend using a calibrated microphone via USB in combination with Multi-Instrument software for the ease of use. We would be pleased to provide technical assistance to those who are interested in establishing this system.

Behavioral assays

Sound-evoked phonotaxis behavior was performed on day 1 adult hermaphrodite worms unless otherwise specified. Animals were tested on NGM plates freshly poured within 1-5 days or stored at 4°C before use. 50 μL of fresh OP50 bacteria was seeded onto the testing plates and dried with the lid off immediately prior to all behavior and calcium imaging experiments. Hermaphrodite worms were transferred to the seeded testing NGM plates 10 minutes before testing to stabilize behavior. Sound was delivered to the worm head or tail using the sound-delivering system described above. We typically stimulated worms with a 2 s pulse of 80 dB SPL sound (1 kHz). No extra hearing protection is necessary when performing such experiments, as only prolonged exposure ($\geq$8 hours) to audible sounds at $\geq$ 85 dB SPL is considered harmful to human ears (Rabinowitz, 2000). As shown in Figure 1A, the output port of the speaker (0.4-0.5 mm inner diameter) was set 0.5 mm above the agar surface. Once the height was set, the output port of the speaker was then aimed at the head or tail of a slowly-moving worm and was positioned at 1-1.5 body lengths away from the worm in the X-Y plane. This was achieved by slowly and gently moving the NGM plate by hand while the speaker was held fixed in place. This protocol did not appear to affect behavior, as the converse experiment, in which we moved the speaker with the manipulator while holding the NGM plate in place, yielded a similar result (Figure S1A). The sound stimulus was carefully calibrated with a mini-microphone (1 mm inner diameter) described above by mimicking the actual experimental conditions. To do so, we placed the mini-microphone on the surface of an NGM assay plate at a location where a worm would normally reside during the behavioral test, and pointed the output port of the speaker at the mini-microphone in a way similar to that described above for the behavioral test. For head-avoidance assays, the response was scored if the worm reversed at least half of one head-swing within 3 s upon the cessation of sound stimulus (typically 2 s pulse of 1 kHz at 80 dB SPL unless otherwise indicated). For tail-avoidance assays, the sound stimulus was directed from the side at the tail of worms who were moving very slowly. A response was scored if upon sound stimulation, the worm increased forward locomotion within 3 s upon the cessation of sound stimulus (2 s pulse, 1 kHz at 89dB SPL). Under the same stimulus condition, the head of the worm appears to be more sensitive to sound than the tail in behavioral tests. To tabulate percent responding, each worm was tested five times with a 10-minute interval between trials. We focused on assaying the head-avoidance response, as it is much easier to score this response.

To assay osmotic avoidance behavior, day 1 hermaphrodite worms were transferred to the testing plates 10 minutes before testing to stabilize behavior. The test was performed by using a glass needle to drop glycerol (2 M in M13) in front of a forward-moving animal on the agar surface. An avoidance response was scored if the worm ceased forward movement and reversed backward at least half of a head-swing upon the worm nose tip reaching the glycerol drop. To quantify percent responding, we tested each worm five times with a 10-minute interval between trials. For both the osmotic avoidance and head-avoidance phonotaxis assays related to *bli* strains, young day 2 animals were used, as *bli* mutants exhibit variable penetrance of blister phenotype at day 1, but exhibit larger and more frequent blisters by day 2 of adulthood. During assays with these strains, care was taken to select worms with large blisters covering the head but not the nose tip.

The tap response was assayed using day 1 hermaphrodite worms on freshly seeded NGM plates (prepared as described for phonotaxis behavior). Briefly, the NGM plate (with lid off) was gently lifted 3 cm above the microscope surface and released to administer

a plate tap. An avoidance response was scored if the worm reversed at least half of one head swing within 3 s of the tap. Percent responding was calculated by testing each worm five times with a 10-minute interval between trials.

Histamine-induced neuronal silencing was performed as previously described (Pokala et al., 2014). Briefly, full-length cDNA encoding *Drosophila* HisCl1 (a gift from Cori Bargmann) was cloned under the *sto-5* or *ser-2(prom3)* promoter to drive expression in FLP or PVD, respectively (Russell et al., 2014; Tsalik et al., 2003), and injected into N2 animals. For behavior assays, NGM plates were treated overnight with either histamine (10 mM) or vehicle (ddH_2O). For testing, plates were freshly seeded with a thin lawn of OP50 bacteria, and worms were allowed to habituate for 10 min before the phonotaxis assay. Laser ablation was performed on L1-L2 larvae using a laser microbeam (Andor) as described previously (Li et al., 2006), and day 1 adult worms were then tested for phonotaxis behavior.

Laser Doppler vibrometry

Contactless surface vibrations were measured using a laser Doppler vibrometer (LDV; OFV-303, Polytec USA) with a spot size of 10 μm. An NI PCI-6123 card was used to measure the LDV response. For all vibration measurements, 55 mm NGM plates were allowed to dry overnight at room temperature and were used immediately or stored in a cold room wrapped in parafilm to prevent desiccation for up to one week. Worms showed normal sound-evoked phonotaxis responses under this condition. To prepare for measurements, a group of five worms were first paralyzed in 10 mM NaN3 (in M13) solution, transferred to an unseeded NGM plate to remove excess liquid, and then moved to a testing NGM plate containing 10 mM NaN3. LDV measurements were taken by focusing the laser beam spot on each worm at the anterior region of the animal right behind the pharynx. The sound stimulus from the speaker output port (1.5 mm inner diameter) was delivered to the worm as described for the behavior assay. For vibration measurements in Figures 2B–2E, day 1 adult worms were used, while for those in Figures 2F and 2G, day 2 worms were analyzed as the penetrance of *bli* mutant phenotype was more pronounced at day 2. During assays with *bli* strains, care was taken to select worms with blisters large enough in the anterior region to allow the laser to focus on the area with a disrupted cuticle. Vibration measurements were taken by acquiring voltage (mm/s/V) for 1 s at a sampling rate of 10 kHz for sound frequencies < 5 kHz, and at a sampling rate of 15 kHz with a 20 kHz velocity filter for sound frequencies ≥ 5 kHz. Voltage data underwent post-processing in MATLAB using custom scripts and a set conversion factor of 10 mm/s/V to obtain displacement and velocity measurements with respect to frequency. Ten measurements were taken for each plate on the anterior regions of the worm body to obtain the worm surface measurements and on the agar surface close to the worms for the agar substrate measurements.

Calcium imaging

Calcium imaging was performed on freely-moving animals using the CARIBN system as previously described (Piggott et al., 2011). Briefly, imaging was performed in an environmentally controlled room (20°C, 30% humidity) on day 1 adult hermaphrodites using assay plates prepared as described for the phonotaxis assay. Hermaphrodite worms were picked one day before the experiment at L4 stage. Prior to testing, worms were transferred to freshly seeded NGM plates 10 minutes before testing. Sound stimulus (10 s) from the output port of the speaker (1.5 mm inner diameter) was delivered using the device described above. The speaker was adjusted to be 0.5 mm above the agar surface using a micromanipulator and at a distance of approximately four body lengths away from the worm. The sound stimulus from the speaker was calibrated as described for the phonotaxis assay using a mini-microphone (1 mm inner diameter) situated in a similar position to the worm on the NGM plate. Ratiometric imaging was performed on worms co-expressing GCamp6(f) and mCherry, and $\Delta R/R$ was used to quantify changes in fluorescence. We quantified the peak calcium response, as peak responses are more consistent between experiments.

Electrophysiology

HEK293T cells were cultured in DMEM medium containing 10% fetal bovine serum (heat inactivated) in a 37°C incubator containing 5% CO2. Cells were transferred into 35 mm dishes one day prior to transfection. *C. elegans* cDNA for *des-2, deg-3* and *ric-3* were cloned into mammalian expression vector pcDNA3. Cells were transfected with Lipofectamine2000 (ThermoFisher) for 4 hours. EGFP and *ric-3* was co-transfected with the genes of interest. EGFP functioned as a marker, and RIC-3 is a chaperone to facilitate DES-2/DEG-3 trafficking to the cell membrane. The DNA amount ratio for *des-2/deg-3/ric-3* was 1:1:1. Cells were recorded at 12∼18 hours post-transfection.

Whole-cell patch-clamping was carried out using an Olympus IX73 inverted microscope with a Multiclamp 700B amplifier. Transfected cells were identified by green fluorescence signal. Choline (10 mM) was diluted in the bath solution and perfused toward the cell using a rapid perfusion system (RSC-200, Bio-Logic). Pipette resistance was 2-5 MΩ when filled with pipette solution. Cell capacitance and series resistance were compensated during recording. Voltage was clamped at −70 mV. Bath solution (in mM): 140 NaCl, 3 KCl, 2 CaCl2, 1.5 MgCl2, 10 glucose, and 10 HEPES (pH adjusted to 7.3). Pipette solution (in mM): 145 KCl, 1 MgCl2, 5 EGTA and 10 HEPES (pH adjusted to 7.2).

Confocal microscopy

Images were captured on a Nikon spinning-disk confocal microscope using a 60x objective as previously described (Wang et al., 2021). Briefly, late L4 or young adult worms were mounted on a 2% agarose pad (in M13) containing 5 mM levamisole to paralyze the worms. Excitation intensity was enhanced to clearly show the quaternary branches, which required slightly over-exposing the

cell body. For each image, approximately 30 Z steps of 0.5 μm/step were taken to ensure all branches of the PVD/FLP neuron could be clearly observed.

QUANTIFICATION AND STATISTICAL ANALYSIS

Statistics were performed using GraphPad Prism. P values < 0.05 were considered significant. The statistical method, error bars, and n number were all described in the figure legends. Specifically, for those involving multi-group comparisons, we applied ANOVA followed by a post hoc analysis. t test was applied to those involving two sample groups.

Neuron, Volume *109*

Supplemental information

The nematode *C. elegans* senses airborne sound

Adam J. Iliff, Can Wang, Elizabeth A. Ronan, Alison E. Hake, Yuling Guo, Xia Li, Xinxing Zhang, Maohua Zheng, Jianfeng Liu, Karl Grosh, R. Keith Duncan, and X.Z. Shawn Xu

Figure S1

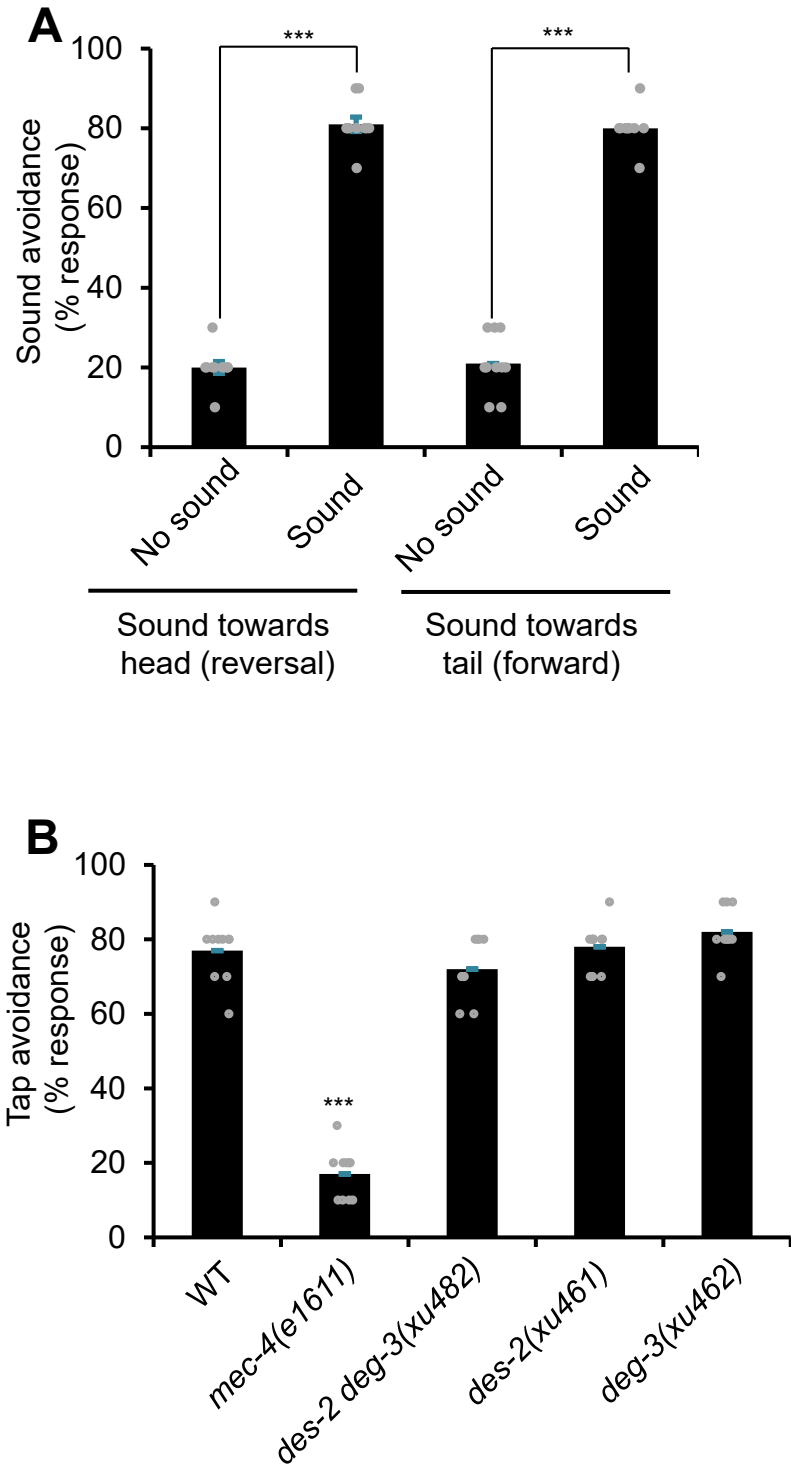

Figure S1. Related to Figure 1. Additional data on phonotaxis behavior and substrate-borne vibration-activated behavior.

(A) Additional data on phonotaxis. In Figure 1C, we tested phonotaxis behavior by slowly and gently moving the NGM plate by hand while the speaker was held fixed in place. Here, we performed the converse experiment by moving the speaker with the manipulator while holding the NGM plate in place. This yielded a similar result . Error bars: SEM. ****p<0.0001(t-test). n≥10.

(B) *mec-4* mutant shows a defect in tap avoidance, while *des-2* and *deg-3* mutant do not. Error bars: SEM. ****p<0.0001 (ANOVA with Bonferroni test). n≥10.

Figure S2

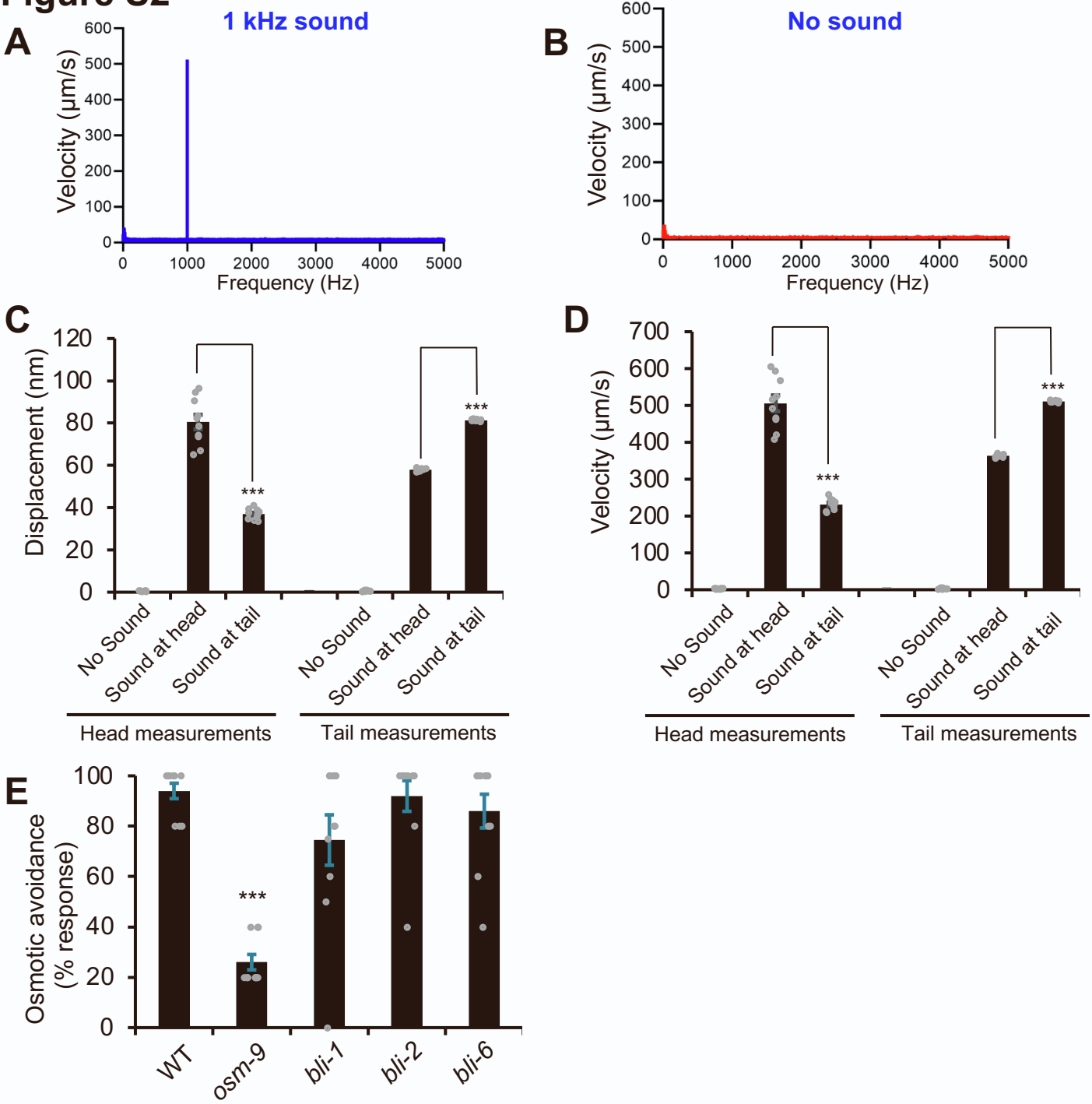

Figure S2. Related to Figure 2. Additional data on sound-evoked cuticle vibrations in WT and cuticle mutants.

(A-B) Worm cuticle vibrates at 1 kHz in response to 1 kHz sound stimulus (80 dB SPL). The small peak near 0 Hz arose from background building vibrations and was present in all recordings, including no sound control.

(C-D) Sound evokes a higher value of cuticle displacement in the head when the stimulus is applied to the head than to the tail, and *vice versa*. Sound stimulus: 1 kHz, 80 dB SPL. Error bars: SEM. ***p<0.0001 (ANOVA with Bonferroni test). n≥10.

(D) *bli* mutants show avoidance response to osmotic stimulus. Worms were tested with glycerol (2 M), which triggered reversals. *osm-9* mutant served as a positive control. Error bars: SEM. ***p<0.0001 (ANOVA with Bonferroni test). n≥10.

Figure S3

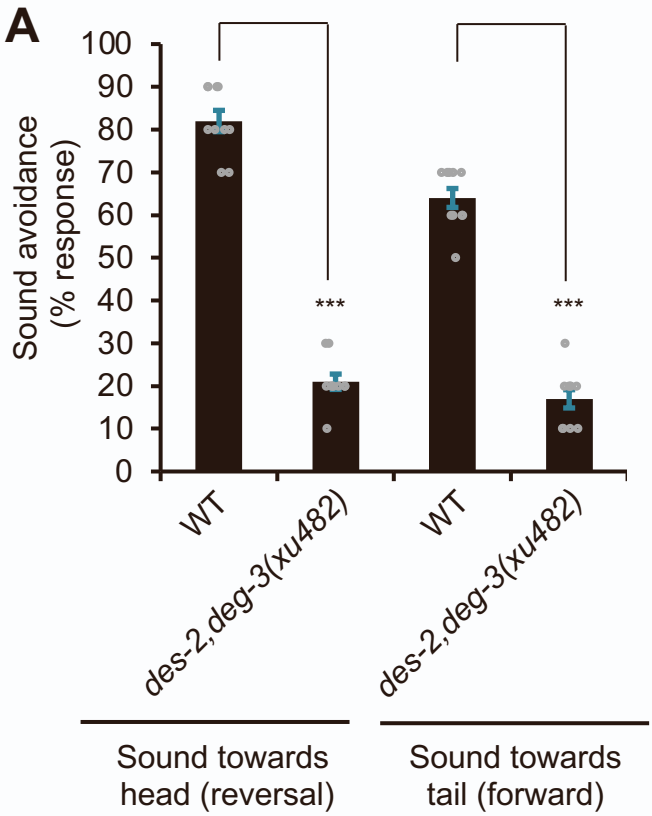

Figure S3. Related to Figure 3. Additional data on phonotaxis behavior. The sound-delivery protocol used for calcium imaging of FLP/PVD neurons is slightly different from that for behavioral measurements, due to the setup of the calcium imaging system (see methods). We thus repeated the behavioral test using the condition adopted for the calcium imaging experiments. The scoring protocol remained the same. We obtained similar results using this protocol in WT worms, and *des-2 deg-3* mutant worms also showed a severe defect under this condition. Error bars: SEM. ****p<0.0001(t-test). n≥10.

Figure S4

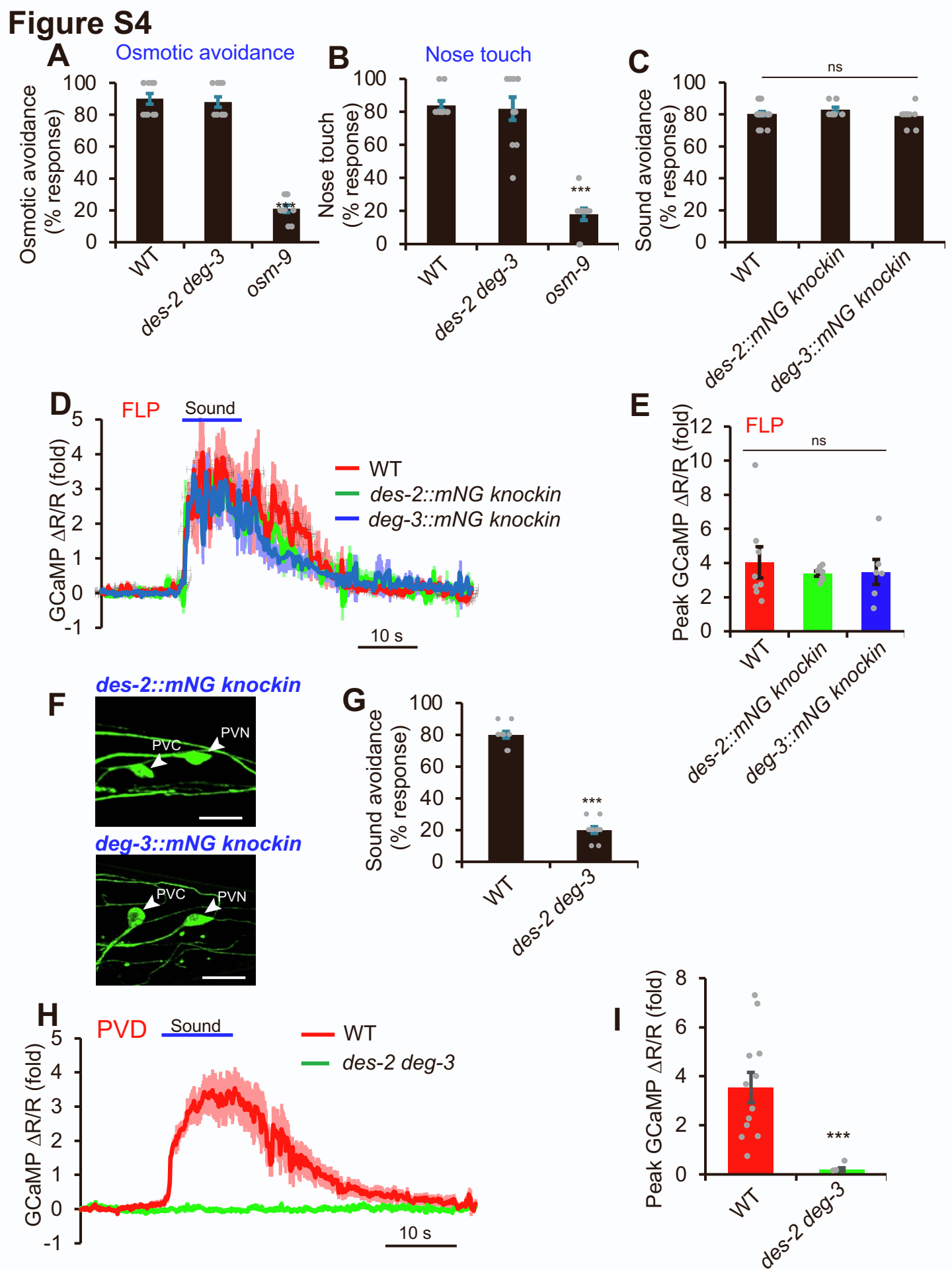
A
Osmotic avoidance
Osmotic avoidance (% response)
WT
des-2 deg-3
osm-9
B
Nose touch
Nose touch (% response)
C
ns
Sound avoidance (% response)
des-2::mNG knockin
deg-3::mNG knockin
D
FLP
Sound
GCaMP ΔR/R (fold)
WT
des-2::mNG knockin
deg-3::mNG knockin
10 s
E
FLP
Peak GCaMP ΔR/R (fold)
F
des-2::mNG knockin
PVC
PVN
deg-3::mNG knockin
G
H
PVD
I

Figure S4. Related to Figure 5. Additional data on *des-2* and *deg-3*

(A-B) *des-2 deg-3(xu482)* mutant worms showed normal osmotic avoidance and nosh touch avoidance behavioral responses. *osm-9* mutant worms, which were defective in both behaviors, were used as a control. Error bars: SEM. ***p<0.0001 (ANOVA with Bonferroni test). n≥10.

(C) *des-2::mNG* and *deg-3::mNG* knockin worms show no defect in phonotaxis behavior. Head-avoidance response was tested. Error bars: SEM. p>0.05 (ANOVA with Bonferroni test). n≥10.

(D-E) *des-2::mNG* and *deg-3::mNG* knockin worms show no defect in sound-evoked calcium responses in FLP neurons. (D) Average traces. Shades along the traces indicate error bars (SEM). (E) Bar graph. Error bars: SEM. P>0.05 (ANOVA with Bonferroni test). n≥10.

(F) *des-2* and *deg-3* are expressed in additional neurons in the tail area. *des-2* and *deg-3* were previously reported to be expressed in IL2 and PVC neurons besides FLP and PVD (Treinin et al., 1998). We did not detect reliable expression of *des-2* and *deg-3* in IL2 neurons in *des-2::mNG* and *deg-3::mNG* knockin worms. However, knockin worms expressed *des-2* and *deg-3* in additional neurons in the tail region (consistent expression in PVC and PVN and inconsistent expression in a few other tail neurons). Scale bars, 10 μm.

(G) *des-2 deg-3(xu482)* mutant worms are defective in sound-stimulated forward movement. Error bars: SEM. ***p<0.0001 (t test). n≥10.

(**H-I)** *des-2 deg-3(xu482)* mutant worms lack sound-evoked calcium responses in PVD neurons. (H) Average traces. Shades along the traces indicate error bars (SEM). (I) Bar graph. Error bars: SEM. ***p<0.0001 (t test). n≥10.

Figure S5

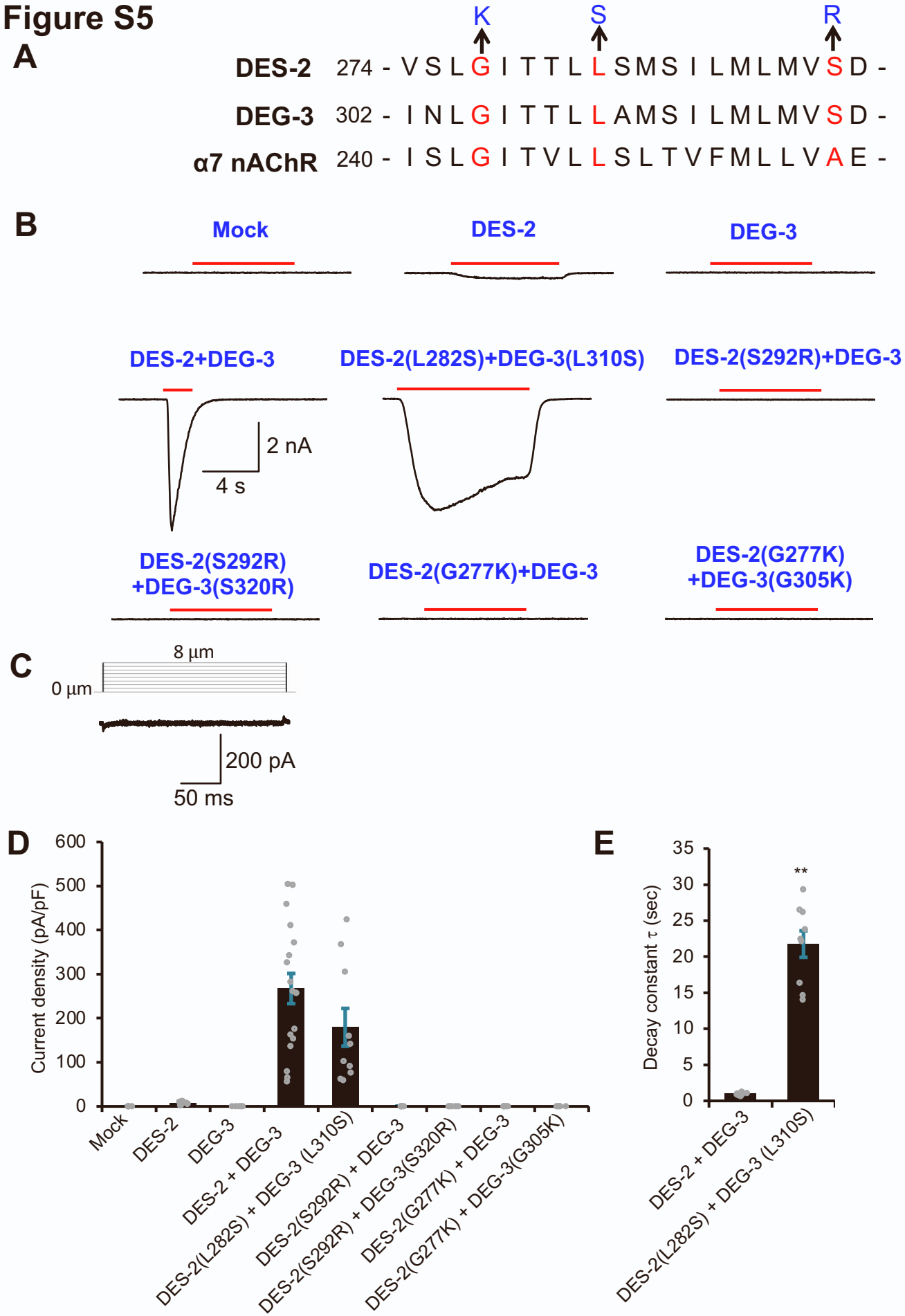
A
K
S
R
DES-2 274 - V S L G I T T L L S M S I L M L M V S D -
DEG-3 302 - I N L G I T T L L A M S I L M L M V S D -
α7 nAChR 240 - I S L G I T V L L S L T V F M L L V A E -
B
Mock
DES-2
DEG-3
DES-2+DEG-3
DES-2(L282S)+DEG-3(L310S)
DES-2(S292R)+DEG-3
2 nA
4 s
DES-2(S292R)
+DEG-3(S320R)
DES-2(G277K)+DEG-3
DES-2(G277K)
+DEG-3(G305K)
C
8 µm
0 µm
200 pA
50 ms
D
Current density (pA/pF)
600
500
400
300
200
100
0
Mock
DES-2
DEG-3
DES-2 + DEG-3
DES-2(L282S) + DEG-3 (L310S)
DES-2(S292R) + DEG-3
DES-2(S292R) + DEG-3(S320R)
DES-2(G277K) + DEG-3
DES-2(G277K) + DEG-3(G305K)
E
Decay constant τ (sec)
35
30
25
20
15
10
5
0
**
DES-2 + DEG-3
DES-2(L282S) + DEG-3 (L310S)

Figure S5. Related to Figure 7. Electrophysiological characterization of wild-type and mutant forms of DES-2/DEG-3 in HEK293T cells.

(A) Sequence alignment of *C. elegans* DES-2 and DEG-3 and human nAChR7 in the pore-lining M2 segment. The residues in DES-2 and DEG-3 that were mutated in this study are marked in red.

(B) Representative current traces from HEK293T cells expressing wild-type and mutant forms of DES-2/DEG-3. Horizontal bars above each trace indicate the application of choline (10 mM), which is known as a potent agonist for DES-2/DEG-3. Agonist was applied to mutant forms of DES-2/DEG-3 for a longer duration to ensure that no current was evoked (for channel-dead mutants) or the current was able to deactivate for a sufficient amount of time needed for data quantification (for L-S mutant). Holding potential: -70 mV. RIC-3, a chaperon for nAChRs, was co-transfected with DES-2 and DEG-3 into HEK293T cells.

(C) No notable mechanically-activated currents were detected in DES-2/DEG-3 expressed in HEK293T cells. Cells were stimulated with a glass probe driven by a piezo actuator as described previously (Li et al., 2011). The stimulus steps, ranging from 0 to 8 μm, were shown to the top.

(D) Bar graph summarizing the data in (B). Mock, DEG-3, DES-2(G277K)+DEG-3, DES-2(S292R)+DEG-3, DES-2(S292R)+DEG-3(S320R), and DES-2(G277K)+DEG-3(G305K) all showed no current (n≥5). DES-2: 8.0±3.4 (pA/pF) (n=10). DES-2+DEG-3: 267.4±145.3 (pA/pF) (n=17). DES-2(L282S)+DEG-3(L310S): 179.5±135.6 (pA/pF) (n=10).

(E) Bar graph showing that DES-2(L282S)/DEG-3(L310S) desensitizes/inactivates more slowly than wild-type DES-2/DEG-3 channel. The decay phase of the currents were fitted with exponential function to calculate the decay constant τ. For DES-2+DEG-3: 0.97±0.19 (s) (n=11); DES-2(L282S)+DEG-3(L310S): 21.76±5.51 (s) (n=9). Data are presented as mean±s.d. ** $p<0.001$ (t test).

Figure S6

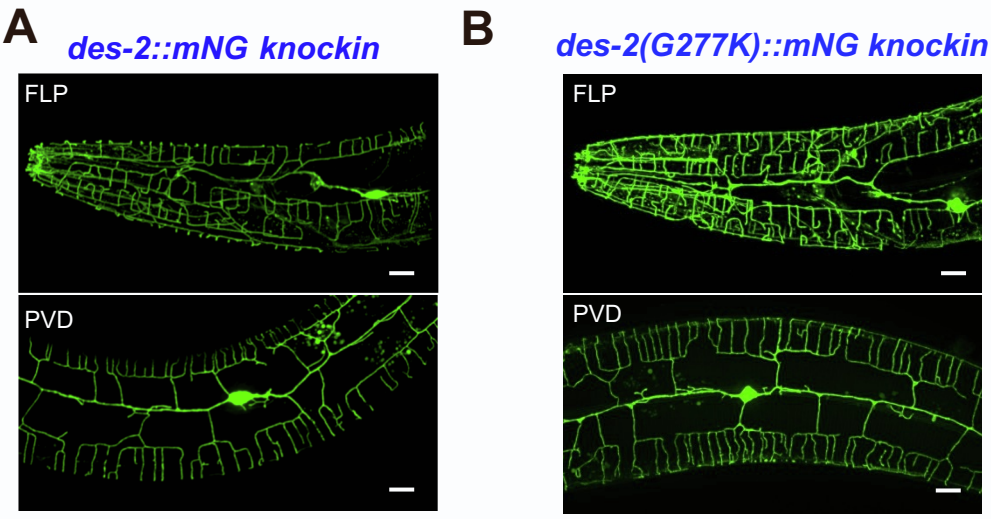

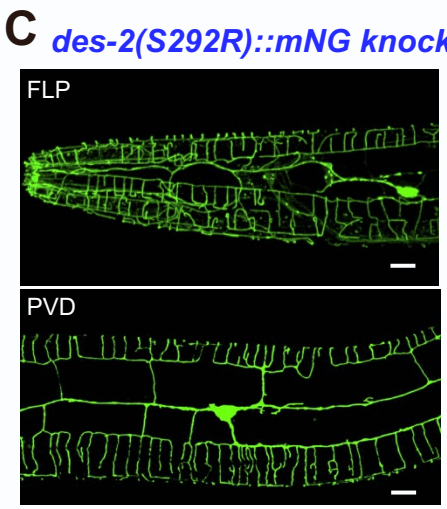

Figure S6. Related to Figure 7. Knockin worms carrying channel-dead mutations show normal expression of DES-2. The channel-dead mutations G277K and S292R were introduced into the endogenous locus of *des-2* by CRISPR-based genome editing. Prior to introducing G277K and S292 point mutations, we first introduced the mNG (mNeonGreen) tag into the endogenous *des-2* locus to produce *des-2::mNG* knockin line by CRISPR-based genome editing. This mNG tag did not affect DES-2 function (Figure S4). We then performed genome editing in this *des-2::mNG* background to introduce the G277K and S292 channel-dead mutations. *des-2(G77K)::mNG* (B) and *des-2(S292R)::mNG* (C) knockin lines show normal expression of DES-2 in FLP and PVD neurons compared to the parental control (A). Scale bars, 10 μm.

Figure S7

A

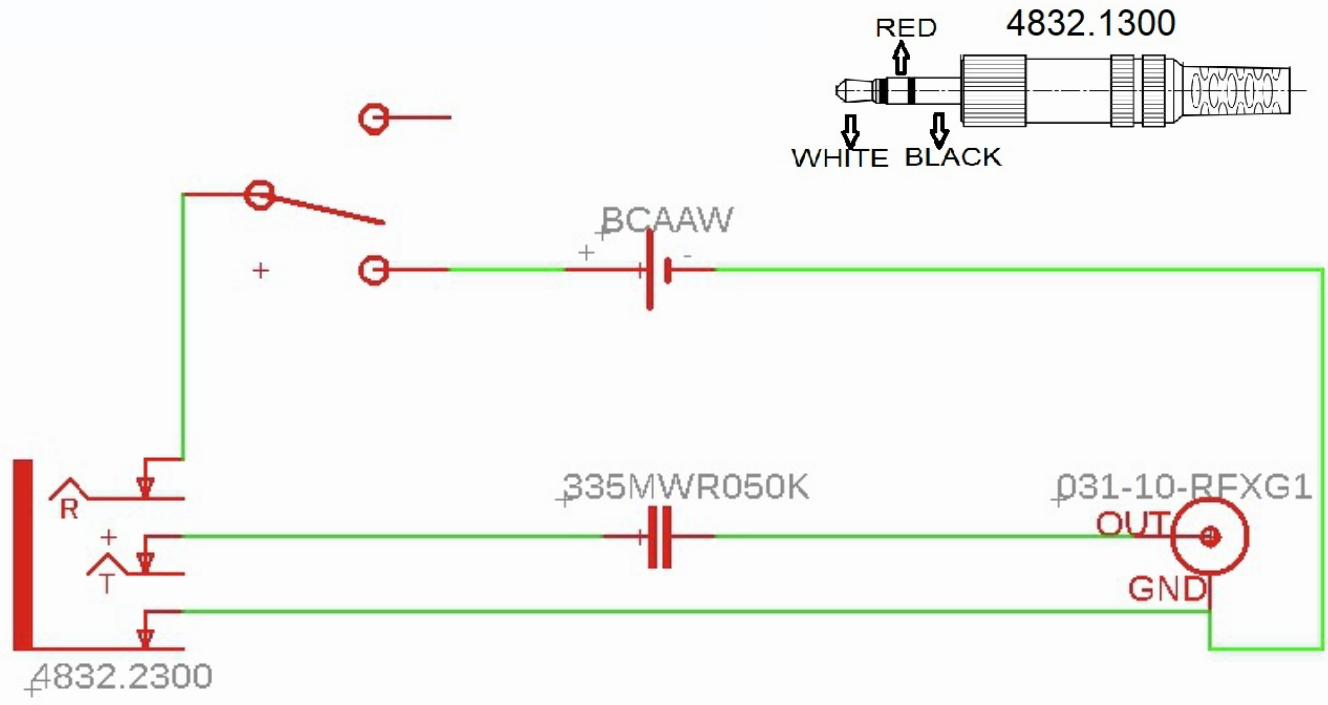

B

Description	Part #	Source
SPDT Toggle switch	M2013SS1W01	Digi-Key Electronics
Panel mount TRS jack	4832.23	Digi-Key Electronics
Metalized film capacitor	335MWR050K	Digi-Key Electronics
AA Battery holder with leads	BCAAW	Digi-Key Electronics
Analog electret condenser microphone	FG-23329-P07	Digi-Key Electronics
TRRS phono cable	10-02153	Digi-Key Electronics
Aluminum enclosure	PRT-13839	Digi-Key Electronics
Panel mount BNC connector	031-10-RFXG1	Digi-Key Electronics
TRS plug (3.5mm)	4832.13	Digi-Key Electronics
BNC to 1/4" audio adapter	1297	Digi-Key Electronics
Focusrite Scarlett solo	SCARLETT-SOLO-3G	B&H Photo Video

Figure S7. Related to Figures 1-7. Schematic and parts list for miniature microphone power supply. The miniature microphone requires its own power supply. (A) A schematic for the design of the custom power supply used to operate the Knowles miniature microphone. (B) The parts list for the items required for assembling the microphone power supply.